Review

Geo-Environmental Models of In-Situ Leaching Sandstone-Type Uranium Deposits in North China: A Review and Perspective

Fuxin Zheng, Yanguo Teng, Yuanzheng Zhai *, Jingdan Hu, Junfeng Dou and Rui Zuo

Engineering Research Center for Groundwater Pollution Control and Remediation of Ministry of Education of China, College of Water Sciences, Beijing Normal University, Beijing 100875, China
* Correspondence: diszyz@vip.163.com

Abstract: Since the 1990s, sandstone-type uranium in the northern basin of China has become the main target for mining. Uranium mining can cause a series of impacts on the environment. A conceptual model of the geo-environment for sandstone-type uranium in northern China was described, which covers the changes in the geo-environmental characteristics in the natural state, in the mining process, during decommissioning and after treatment. Sandstone-type uranium is mainly distributed in the Songliao, Erlian, Ordos, Turpan–Hami and Ili Basins, which have arid climates and poor stratum permeability. Pitchblende is the main uranium-bearing mineral and is associated with iron, copper, coal, organic matter and other minerals. The mineral often has a low ore grade (0.01–1.0%) and high carbonate content (2–25%). Uranyl carbonate accounts for more than 90% of the total uranium in groundwater. The uranyl content is closely related to the TDS. The TDS of groundwater in the eastern and central ore belts is usually lower than 2 g/L, while in the western region, such as Xinjiang, it can exceed 10 g/L. In situ leaching (ISL) is the main mining method that results in groundwater pollution. Acid leaching leads to a pH decrease (<3), and heavy metals represented by U and Fe exceed the background values by hundreds of times, resulting in groundwater pollution. CO_2 leaching is more environmentally friendly, and the excess ions are usually Ca^{2+}, Mg^{2+}, NO_3^- and HCO_3^-. Soil chemical anomalies originate mostly from wind erosion and precipitation leaching of decommissioned tailings. Uranium pollution is mainly concentrated within 20 cm of the surface, and the exceedance generally varies from two to 40 times. During ISL, a series of environmental measures will be taken to prevent pollution from being exposed to the surface. After treatment, the decommissioned uranium mines will likely have no impact on the surrounding environment. In the future, the protection of groundwater should be strengthened during production, and remediation methods based on electrokinetic, microbial and permeable reactive barrier (PRB) technology should be further researched.

Keywords: sandstone-type uranium; geo-environmental model; environmental properties; geochemical baseline; environmental impact; northern China

1. Introduction

As the world's largest carbon-emitting economy, the Chinese government has pledged to achieve carbon neutrality by 2060. To achieve this goal, the number of nuclear power plants in the next 30 years will be increased five times on the current basis [1]. Uranium is the main raw material for nuclear power generation, and the development of nuclear power is bound to significantly increase the mining of uranium [2,3]. The largest reserve uranium deposits in China are sandstone-type deposits, which account for approximately 43% of the total [4]. Since the 1990s, with the introduction of the in situ leaching (ISL) mining method, sandstone-type uranium in northern China basins has gradually replaced southern granite-type and volcanic-type uranium and has become the main mining body [5,6]. Compared with open pit mines, the ISL of uranium is mainly conducted underground, which is relatively friendly to the environment, especially in the atmosphere and soil. However, ISL

often pollutes groundwater due to the use of geological drilling and chemical solvents [7,8]. In addition, heap leaching of tailings poses potential environmental threats [9–11].

A geo-environmental model is a collection of multiple conceptual models that contain information on geology, hydrogeology, geochemistry, engineering, etc. [12]. In 1998, the U.S. The Department of the Interior and the Federal Geological Survey first systematically described the concepts on their web pages and used the host deposit types as the main index to classify environmental models [12,13]. The construction of geo-environment models can provide reference targets and ideas for mine environment management and remediation [12–14]. Uranium deposits usually show some special hydrogeological and geochemical characteristics [15–17], which usually change during and after mining [18,19]. How to repair the geo-environment according to these changes presents new challenges for researchers.

Based on the above, this article describes geo-environmental models of sandstone-type uranium in northern China, which covers the changes in the Earth's environment before, during and after mining, and discusses the prospects of geo-environmental protection and restoration methods in the future. Section 2 describes the distribution of sandstone-type uranium in northern China and summarizes the Earth's environmental characteristics and baselines of these deposits. Section 3 concentrates on the soil, rocks and groundwater chemical anomalies, as well as radiation and vegetation environment changes. The environmental measures during and after mining are addressed in Section 4. Finally, Section 5 provides suggestions for the geo-environmental protection and remediation of sandstone-type uranium mine development.

2. Environmental Properties and Geochemical Baselines

2.1. Environmental Properties

Most of the sandstone-type uranium deposits in northern China are located in arid or semiarid areas [20]. The main ore belts are the Songliao Basin, Erlian Basin, Ordos Basin, Turpan-Hami Basin and Ili Basin from east to west (Figure 1) [21–23]. The largest deposit is Nuheting, located in the Erlian Basin, with a reserve of more than 50,000 t. There are more than ten medium-scale deposits of more than 3000 t. Limited by technical conditions and economic factors, scaled mining is currently mainly concentrated in the Mengqiguer area of the Ili Basin and Qianjiadian area of the Songliao Basin. Uranium ore is usually low-consolidated sandstone composed of detritus of different sizes. The main components of the detritus are quartz and feldspar, and there are also some cemented substances (such as calcareous cement) [24–28]. The ore has a high carbonate content and is rich in organic matter and other reducing substances (such as organic carbon, H_2S and CH_4), which have good reducing abilities [29].

The stratigraphic chronology of uranium deposits varies by region (Figure 2a). Affected by interlayer oxidation, the distribution of ore belts can be divided into oxidation zones, transition zones and primary zones, among which the transition zone is the main metallogenic zone (Figure 2b) [30]. The oxidation zone is mainly associated with pyrite, limonite or siderite. Therefore, the ore is dark yellow or brown, and some ore may even contain "red layers," whose main component is iron oxide [31–33]. In the reduction zone and transition zone, ores are generally gray due to iron reduction (Figure 2) [4,34–36]. In the Ordos and Ili basins, uranium deposits are often associated with coal or copper mines. Paragenesis of uranium and coal is also one of the main resource development methods in these areas [37–40]. Other minerals, such as trace elements and rare earth elements, are usually characterized by abnormal abundance and have higher contents than other ores [41–43]. The main component of uranium minerals is pitchblende [27,28,44,45], while in the Turpan-Hami Basin, the U-bearing minerals are brannerite and coffinite [46]. Uranium minerals are usually found in the crevices of ore and cementitious material and are often associated with hematite and pyrite [45].
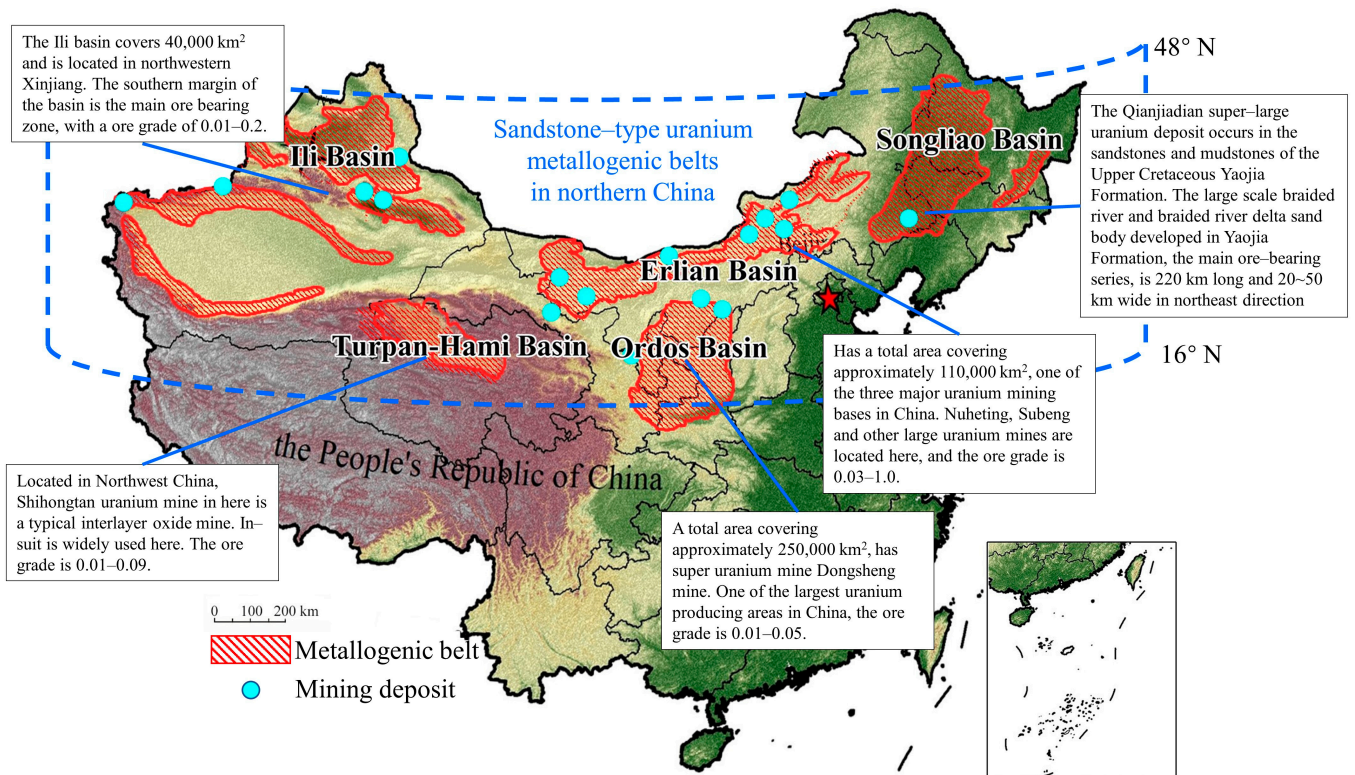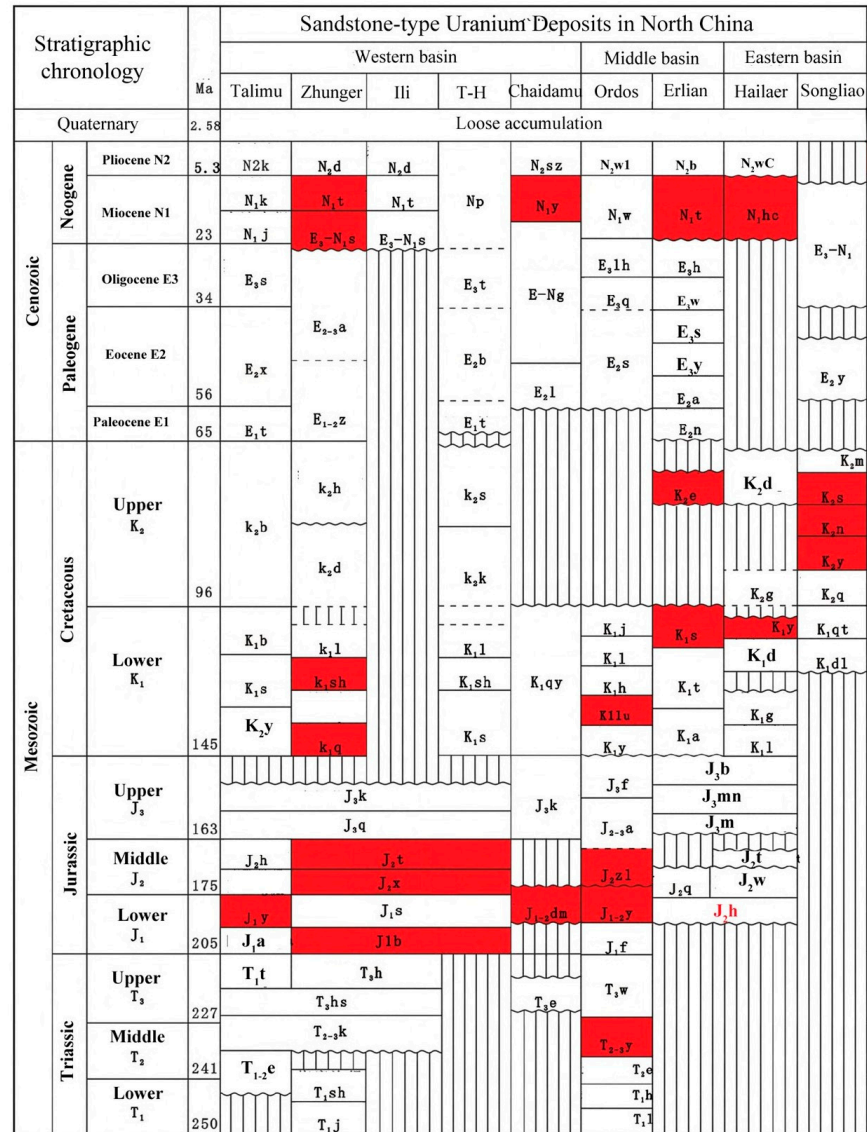
The Ili basin covers 40,000 km² and is located in northwestern Xinjiang. The southern margin of the basin is the main ore bearing zone, with a ore grade of 0.01–0.2.

The Qianjiadian super–large uranium deposit occurs in the sandstones and mudstones of the Upper Cretaceous Yaojia Formation. The large scale braided river and braided river delta sand body developed in Yaojia Formation, the main ore–bearing series, is 220 km long and 20~50 km wide in northeast direction

Sandstone–type uranium metallogenic belts in northern China

Located in Northwest China, Shihongtan uranium mine in here is a typical interlayer oxide mine. In–suit is widely used here. The ore grade is 0.01–0.09.

Has a total area covering approximately 110,000 km², one of the three major uranium mining bases in China. Nuheting, Subeng and other large uranium mines are located here, and the ore grade is 0.03–1.0.

A total area covering approximately 250,000 km², has super uranium mine Dongsheng mine. One of the largest uranium producing areas in China, the ore grade is 0.01–0.05.

Metallogenic belt

Mining deposit

Figure 1. Distribution of sandstone-type uranium deposits in northern China.

Multilayer aquifer systems are universal in all these deposits [47–50]. For example, the Qianjiadian uranium deposit in the Songliao Plain has four aquifers with an average thickness of 55 m [48], and the Shihongtan deposit in the Turpan-Hami Basin has seven aquifers with an average thickness of approximately 23 m [49]. The aquifer is often composed of light gray or reddish gravelly sandstone mixed with argillaceous cementation. Dense and continuous groundwater barriers are usually composed of mudstone with a thickness of 1–6 m [47–50]. These aquifers determine the ore occurrence characteristics through the control of redox conditions and then affect the geo-environment of the deposits (Figure 3). Similar to the metallogenic differences between the eastern and western Shihongtan ore belts [51], the uranium occurrence differences in the northern and southern Ili Basin [50] are all related to the interlayer oxidation of groundwater.

Precipitation is the main source of groundwater [36,47]. In Northwest China (Ili and Turpan-Hami Basins), there is also Quaternary phreatic recharge from mountains in the basin margins [50,52]. Controlled by the tectonic system and geological conditions, the groundwater flows from the basin edge to the central depression. The hydraulic gradient and flow velocity vary from different basins. In open basins (Songliao, Erlian or Ordos Basin), the hydraulic gradient is generally less than 2‰, and the groundwater flow velocity is low. Similar to the Erlian Basin, the hydraulic gradient is 0.3–1.4‰, and the groundwater flow velocity is 0.7–2.9 m/a. In intermountain basins, the hydraulic gradient is generally 4–5‰, and the groundwater velocity can reach approximately 4 m/a [53]. This value will be higher in areas with large local topographic fluctuations, such as the No. 513 mine in Sudongbulake and the No. 510 mine in Honghaigou, where the hydraulic gradient reaches 7–9‰ and 23–35‰, respectively. The groundwater flow velocity exceeds 17 m/a [53]. Due to the arid climate, groundwater discharge is usually dominated by evaporation [47,54,55]. Except for the Shihongtan area in the Turpan-Hami Basin, the groundwater in most deposits is of good quality, with low salinity and moderate to weakly alkaline pH. Ca^{2+}, Na^+, HCO_3^-, SO_4^{2-} and Cl^- are the main ions [38,47,53,56]. These ions come from rock dissolution (such as gypsum and calcite) under water-rock interactions. In addition to conventional ions, groundwater also contains sulfides (such as H_2S, HS^-,

S^{2-}, etc.), reducing gas (such as CH_4), Fe^{3+}/Fe^{2+}, and some trace elements [57–59]. Uranium in groundwater often exists in the form of uranyl. U(VI) is dominant in the oxidation environment of shallow aquifers, while U(IV) is dominant in deep reduction aquifers [47,52,60]. The formation of the Ili uranium deposit is due to uranium valence changes in different aquifers. Uranium in the shallow aquifer is continuously oxidized and enters groundwater in the form of uranyl [such as $UO_2(CO_3)_2^{2-}$ and $UO_2(CO_3)_3^{4-}$] (Table 1). The uranyl enters the deep aquifer with the recharge and flow of groundwater, where uranyl is restored to U (IV) precipitation and mineralization [50,55].
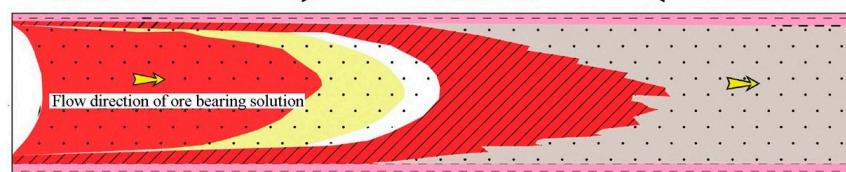
(a)

Stratigraphic chronology			Ma	Sandstone-type Uranium Deposits in North China								
				Western basin					Middle basin		Eastern basin	
				Talimu	Zhunger	Ili	T-H	Chaidamu	Ordos	Erlian	Hailaer	Songliao
Quaternary			2.58	Loose accumulation								
Cenozoic	Neogene	Pliocene N2	5.3	$N2k$	N_2d	N_2d		N_2sz	N_2w1	N_2b	N_2wC	
		Miocene N1	23	N_1k / N_1j	N_1t / $E_2\text{-}N_1s$	N_1t / $E_2\text{-}N_1s$	Np	N_1y	N_1w	N_1t	N_1hc	$E_3\text{-}N_1$
	Paleogene	Oligocene E3	34	E_3s			E_3t	$E\text{-}Ng$	E_31h / E_3q	E_3h / E_3w / E_3s		
		Eocene E2	56	E_2x	$E_{2\text{-}3}a$		E_2b	E_21	E_2s	E_3y / E_3a		E_2y
		Paleocene E1	65	E_1t	$E_{1\text{-}2}z$		E_1t			E_2n		
Mesozoic	Cretaceous	Upper K2	96	k_2b	k_2h / k_2d			k_2s / k_2k	K_2e / K_2g	K_2d		K_2m / K_2s / K_2n / K_2y / K_2q
		Lower K1	145	K_1b / K_1s / K_2y	k_1l / k_1sh / k_1q	K_1l / K_1sh / K_1s	K_1l / K_1sh / K_1s	K_1qy	K_1j / K_1l / K_1h / $K1lu$ / K_1y	K_1s / K_1l / K_1t / K_1a	K_1y / K_1d / K_1g / K_1l	K_1qt / K_1d1
	Jurassic	Upper J3	163		J_3k / J_3q			J_3k	J_3f / $J_{2\text{-}3}a$		J_3b / J_3mn / J_3m	
		Middle J2	175	J_2h	J_1t / J_1x	J_1t / J_1x			J_2zl	J_2q	J_2t / J_2w	
		Lower J1	205	J_1y / J_1a	J_1s / $J1b$	J_1s / $J1b$		$J_{1\text{-}2}dm$	$J_{1\text{-}2}y$ / J_1f		J_1h	
	Triassic	Upper T3	227	T_1t	T_3h / T_3hs			T_3e	T_3w			
		Middle T2	241	$T_{1\text{-}2}e$	$T_{2\text{-}3}k$				$T_{2\text{-}3}y$ / T_3e			
		Lower T1	250		T_1sh / T_1j				T_1h / T_1l			

Oxidation zone →   Transition zone   ← Reduction zone

(b)

Flow direction of ore bearing solution

Dark altered sandstone   Light altered sandstone   Fade altered sandstone   Uranium ore   Original sandstone   Interlayer

Figure 2. Stratigraphic chronology of stone-type uranium deposits in northern China (**a**) and a sketch of the oxidation-reduction zone (**b**) in the metallogenic belt. T-H means Turpan-Hami Basin.

Table 1. Hydrochemical baseline of the representative ore belt in each region.

Area	Location	Water Type	Hydrochemical Type	pH	TDS (mg/L)	Uranyl Types	Concentration of U (µg/L)	References
Songnen Basin	Qianjiadian	Confined groundwater of Yaojia Fm	$HCO_3 \cdot$ Cl-Na, Cl$\cdot$HCO$_3$-Na	7.15–7.79	3.64–4.12	$UO_2(CO_3)_3^{4-}$, $UO_2(CO_3)_2^{2-}$	130–312	[48,61]
Erlian Basin	Yihegaole	Bedrock fissure water	$HCO_3 \cdot SO_4$-Na$\cdot$Mg, $HCO_3 \cdot SO_4$-Na$\cdot$Ca	7.12–10.87	<2000	$UO_2(CO_3)_3^{4-}$, $UO_2(CO_3)_2^{2-}$	0.02–244	[62]
Ordos Basin	Northern basin	Surface water	/	9.31–9.32	412–3710	/	1.14–1.18	[47]
		Jurassic confined water	$SO_4 \cdot$Cl-Na	8.58–12.34	157–1060	$UO_2(OH)_3^-$, $UO_2(CO_3)_3^{4-}$, $UO_2(OH)_2$	0.44–1120	
Turpan-Hami Basin	Southern Shihongtan	Bedrock fissure water	Cl$\cdot SO_4$-Na, Cl-Na, SO_4-Ca$\cdot$Mg	8.02–8.25	8250–12,160	$UO_2(CO_3)_3^{4-}$, $UO_2(CO_3)_2^{2-}$	44.5–4237	[51,52]
Ili Basin	South edge of the basin	Jurassic interlayer porous confined water	HCO_3-Ca, HCO_3-Ca$\cdot$Na, $HCO_3 \cdot SO_4$-Na$\cdot$Ca, $SO_4 \cdot HCO_3$-Ca$\cdot$Na, $SO_4 \cdot$Cl-Na$\cdot$Ca	7.8–8.5	50–2790	$UO_2(CO_3)_3^{4-}$, $UO_2(CO_3)_2^{2-}$	10–1200	[50,55]
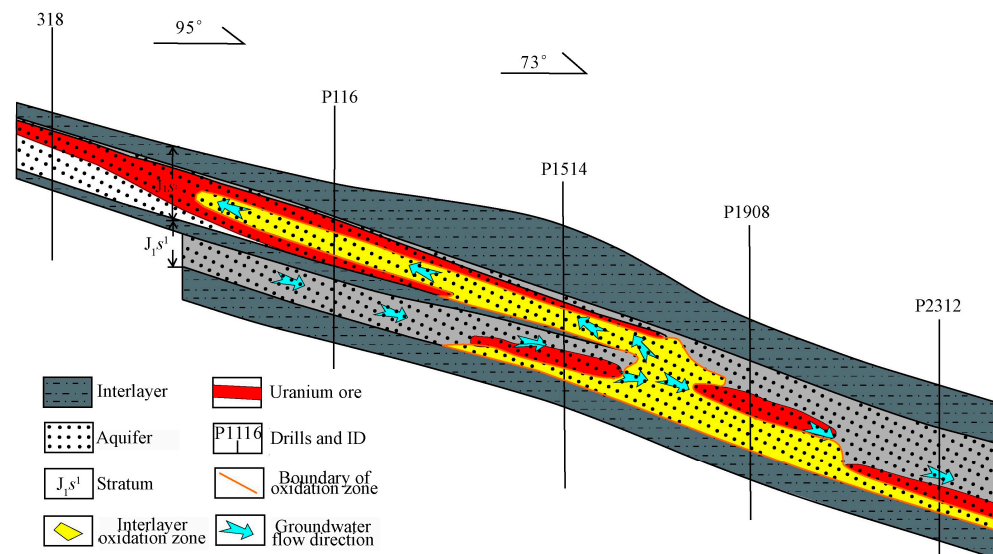
Figure 3. Aquifer and interlayer oxidation in the metallogenic belt.

2.2. Geochemical Baseline

The geochemical baselines in different regions are shown in Table 2. The proportion of detritus in the ore is generally more than 80%, and the detritus is composed of more than 60% quartz [26,63,64]. Approximately 90% of the ores have a carbonate content of 1–3% (carbonate-containing ores), and a few can reach more than 3% (carbonate ores) [65–68]. Some ore carbonate contents in the Ili Basin can reach up to 5–25% [64,69,70]. The uranium grade of the ore is generally between 0.01–0.05%. The Ili Basin has the highest average level in the phreatic oxidation zone of the southern basin margin (0.1–0.2%) and in the coal seam (88.7 µg/g) [27]. Approximately 70–90% of uranium minerals are UO_2. The pH of the metallogenic belt (transition zone) is nearly neutral to weakly alkaline, and the organic matter is generally 0.1–1.5% [65]. The Songliao Basin has the lowest organic matter content, with an average of only approximately 0.2%, while the Ordos Basin has the highest organic matter content, and some ores can reach 5–10% [28,68].

Table 2. Geochemical baselines of representative ore belts in each region.

Area	Location	Ore Types	Grade (%)	Lithic Fragments Ratio (%)	Carbonate Content (%)	Organic Matter Content (%)	Associated Minerals	Enriched Trace Elements	References
Songnen Basin	Qianjiadian	Coarse brownish red feldspathic sandstone, fine–coarse gray sandstone, red mudstone	0.01–0.03	90	2	Ave: 0.2 Max: 1.0	Pyrite, siderite	V, Cr, Co, Ni, Zn	[26,36,66,68]
Erlian Basin	Nuheting	Dark gray silty mudstones, siltstone	0.03–1.0	60–90	1.9	0.1–0.82	Pyrit	V, Mo, Cu, Pb, Zn, Se, Ni	[34,63]
Ordos Basin	Nalinggou	Red, green and gray mudstones, siltstones and sandstones	0.01–0.05	80–90	2.67	Ave: 0.5 Max: 5–10	Coal, pyrite, chalcopyrite	Rb, Ba, Th, K, Pb	[28,65,70]
Turpan-Hami Basin	Shihongtan	Gray white, light gray, light brown, yellow sandstone	0.01–0.09	20–50	2–3	0.1–1.5	Pyrite	V, Se, Mo, Re	[56,67,71]
Ili Basin	South edge of the basin	Gritstone, gravel sandstone, sandstone, siltstone, mudstone, and coalstone	0.01–0.2	46–79	5–25	0.1–2.8	Pyrite, coal	As, Ag, Sb, Se, Fe, S, Mo	[64,69,72]

The associated trace elements in ores of different regions have similarities and differences in element types and enrichment (Figure 4). For example, the main associated trace elements in the Songliao and Erlian Basins are Re, Th, Ba, Se, Co, Ni, Pb, V, Zn, etc., but the Songliao Basin has a stronger enrichment effect [43,73]. The ores in the Dongsheng mine (Ordos Basin) and No. 511 mine (Ili Basin) are both associated with and enriched with Se, Mo and Ge [24,25]. However, the No. 511 mine is additionally associated and enriched with Re and V. The contents of Se and Re in the No. 511 mine are higher, and the ore has a comprehensive utilization value, which is not available in the Dongsheng mine [42]. In addition, rare earth elements (REEs) are usually high in the Erlian Basin and the Ordos Basin. The $\sum$REE contents in the Dongsheng mine are 94.29×10^{-6}~203.53×10^{-6}, while those in the Bayintala mine are 105.01×10^{-6}~169.80×10^{-6} [74].
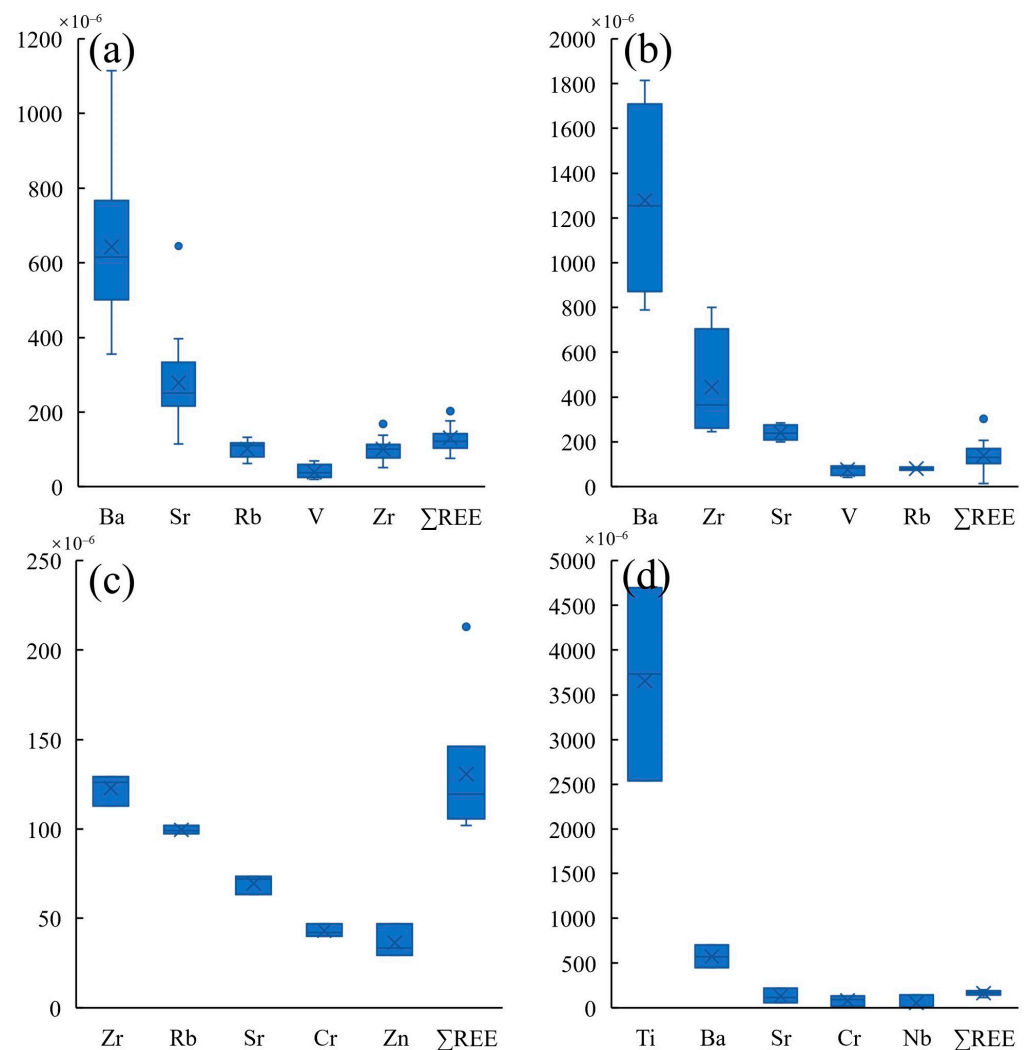
Figure 4. Statistics of the main trace elements and $\sum$REEs in each ore zone (10^{-6}) (**a**) for Qianjiadian in the Songliao Basin; (**b**) for Dongsheng in the Ordos Basin; (**c**) for Shihongtan in the Turpan-Hami Basin; and (**d**) for the southern edge of the Ili Basin [38,41,54,75–78].

The location of uranium deposits usually shows some hydrochemical anomalies (Figure 5). These chemical differences can be used as prospecting indicators for uranium deposits in the area and provide a reference for subsequent mining. The hydrochemical baselines of the same area show differences due to the different groundwater occurrences and types (Table 2). In the Songliao Basin, the groundwater chemical type in the upper aquifer is $HCO_3 \cdot Cl$-Na, the TDS is approximately 580 mg/L, and the pH is 7.65. The groundwater in the lower aquifer has better quality than that of the upper aquifer, and

it can reach class III for the "standard for groundwater quality (GB/T 14848-2017). The groundwater chemical type is $HCO_3 \cdot Cl-Na$ and $Cl \cdot HCO_3-Na$, the TDS is approximately 3.64–4.89 mg/L, and the pH is 7.15–7.79 [48]. In the Erlian Basin, the bedrock fissure water in the low mountain area is mostly $HCO_3-Ca \cdot Na$ type water, and the TDS is less than 2000 mg/L. The bedrock fissure water in the hilly area is the $HCO_3 \cdot SO_4-Na \cdot Mg$ type or $HCO_3 \cdot SO_4-Na \cdot Ca$ type, the TDS is generally greater than 1000 mg/L, and some parts are as high as 2000–4000 mg/L. The pore water quality is mainly affected by evaporation and concentration, which increases the TDS of groundwater. From upstream to downstream, evaporation and concentration become stronger, and the TDS changes from low to high. The water type downstream is Cl-Na, and the TDS significantly exceeds 4000 mg/L [62]. The shallow groundwater (<20 m) in the northern Ordos Basin is of the HCO_3-Ca and $HCO_3-Ca \cdot Mg$ types, the pH is 7.53–8.06, and the TDS is 126–497 mg/L. Deep Cretaceous confined water with good quality ranges from 28 m to 300 m, and the TDS is 877–968 mg/L, which supplies local people and livestock drinking water [47]. The shallow groundwater in the Ili Basin is mainly the $SO_4 \cdot Cl-Na \cdot Ca$ type, and the TDS is low (<500 mg/L) or medium (500–5000 mg/L) [50,55]. The groundwater in the Turpan-Hami Basin has a high TDS, the deposit aquifers are mainly Cl SO_4-Na type water (TDS: 8–12 g/L), and the anticline area of the southern deposit is Cl-Na type water (TDS > 12 g/L) [52].
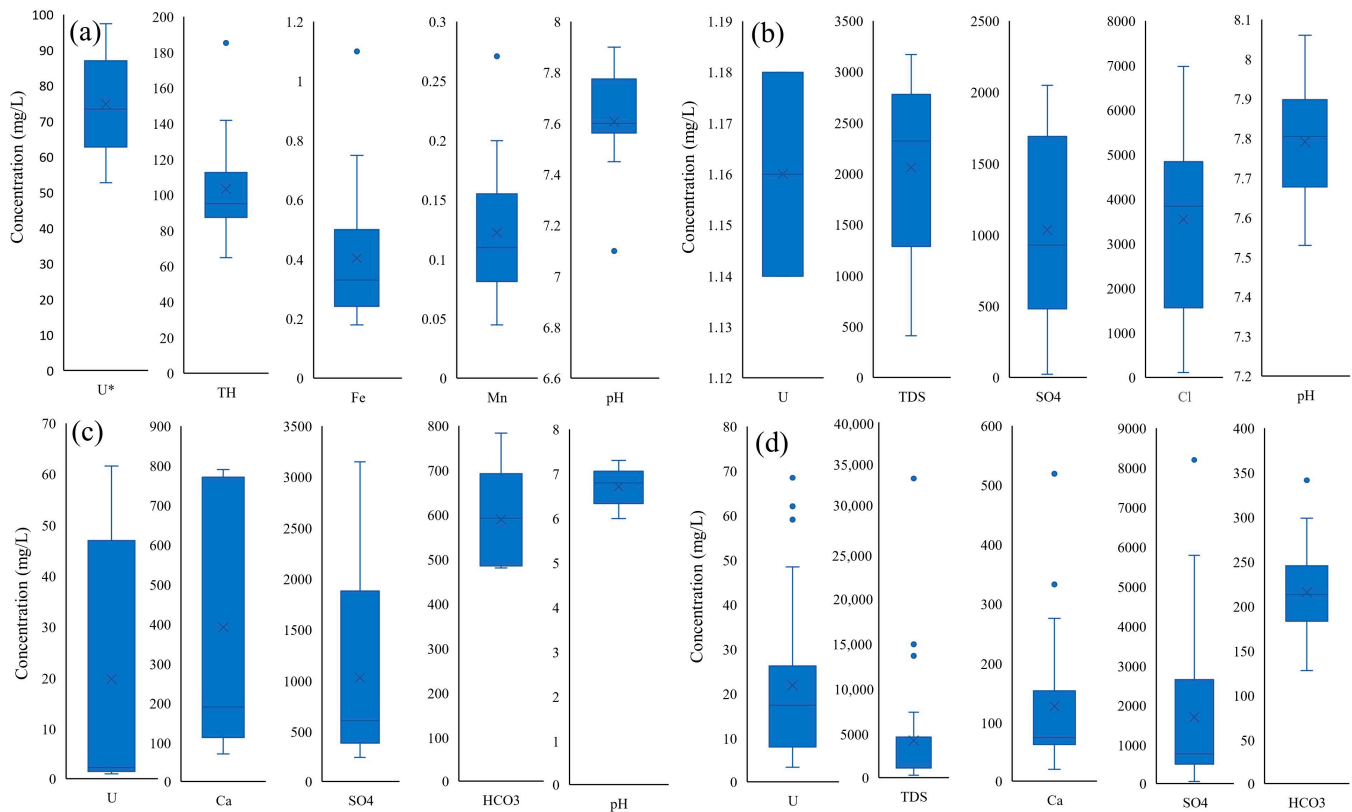
Figure 5. Representative constant elements of groundwater in the ore belt (**a**) for the Songliao Basin; (**b**) for the Ordos Basin; (**c**) for the Turpan-Hami Basin; and (**d**) for the Ili Basin. The pH is unitless, and * represents μg/L [14,75,79–91].

More than 90% of the uranium in groundwater is uranyl carbonate, followed by uranyl hydroxide [47,60]. The U content in groundwater is positively correlated with the U content in rocks [47,60]. In Shihongtan, Turpan-Hami Basin, the U content in the groundwater of the southern deposit (uranium-rich ore) is 44.5–4237 μg/L, while in the northern deposit (uranium-poor ore), the highest U content in the groundwater is only 65.1 μg/L, with an average of 29.3 μg/L [52]. In addition, the U content in groundwater is negatively correlated with TDS. In the Songliao Basin, the average U concentration in the upper aquifer

with high TDS is approximately 4.6 µg/L and that in the lower aquifer with low TDS is 130.0–312.0 µg/L [48]. In the southeastern Alanor area, Erlian Basin, the groundwater discharge has high TDS, and the uranium concentration is 0.021–244 µg/L, while in the Nuheting area, which has low TDS, the concentration of U can reach 453 µg/L [92]. In the Ili Basin, the uranium concentration in $SO_4 \cdot Cl$-Na-type water with high TDS is generally less than 10 µg/L, while in $HCO_3 \cdot SO_4$-Ca-type water with low TDS, it is more than 30 µg/L [50,55] (Table 1).

Surface water in sandstone-type uranium deposits is often of poor quality, and the water-rock interaction with uranium ore is small. For example, studies on streams and lakes in northern Ordos [47] found that the local surface water is weakly alkaline, with a pH of approximately 9.3. The TDS is 412–3710 mg/L, approximately 6.4 times that of groundwater at the same location. The main ions in water are Na^+, Mg^{2+} and HCO_3^- and Cl^-. The U concentration is 1.14–1.18 µg/L, which is only approximately 1/24 of the groundwater. There are no significant differences between uranium ore belts and other places for surface water. Compared with groundwater, uranium ore does not significantly affect the quality of surface water.

3. Environmental Impact of Uranium Mining and Extraction

3.1. Overall Characteristics of Environmental Impact

In situ leaching (ISL) of uranium directly injects the solvent into the underground mining layer and extracts uranium minerals through the reaction between the solvent and ore [93,94]. The most common ISL method is acid leaching, which dissolves and mines uranium by injecting $H_2SO_4 + H_2O_2$ [94,95]. Secondly, in the Songliao, Ordos and Ili Basins, the alkaline method (or CO_2 method, $CO_2 + O_2$, weakly alkaline) has also been adopted [28,96]. Compared with open-pit mining, ISL has limited surface impact but a noticeable effect at depth [96]. Therefore, the mining process and tailings have a certain impact on the water and soil environment in and around the mine.

The pH of the deposits and groundwater are usually near-neutral. Acid leaching leads to pH reduction because of H_2SO_4 pollution. Meanwhile, leaching leads to the dissolution and release of other minerals, such as pyrite, which releases Fe^{3+} into the groundwater. Fe^{3+} as an oxidant further increases the release of other metal or alkali metal ions [94,95]. In alkaline leaching, CO_2 reacts with carbonates, resulting in an increase in Ca^{2+} and Mg^{2+}. Other heavy metals are also released by mineral dissolution. However, due to the near-neutral environment, insoluble metal sediment is formed quickly, so the content of heavy metal ions in groundwater is low [28,96].

3.2. Environmental Impacts on Soil

Soil chemical anomalies usually originate from eroding and leaching tailings rather than production (Figure 6). Wind-borne pollution and water leaching are the main sources of pollution [79]. Wind propagation affects a wide range, but pollution is generally only distributed on the soil surface. For example, in a U-Th tailing in northern China [83], the radioactive elements U and Th were abnormally high in the southeast of the tailing due to the prevailing northwest wind. The content of U in the downwind soil was 2.65 times the background value and 1.61 times the upwind value. The soil pollution from tailings spread to approximately 4 km but was basically distributed within 10 cm of the surface. The water leaching range is small, but the vertical effect is deeper. For example, in a tailing pond [97], the U content reached its peak at 8.5 m from the surface due to perennial precipitation leaching. The maximum migration depth reached 14 m.
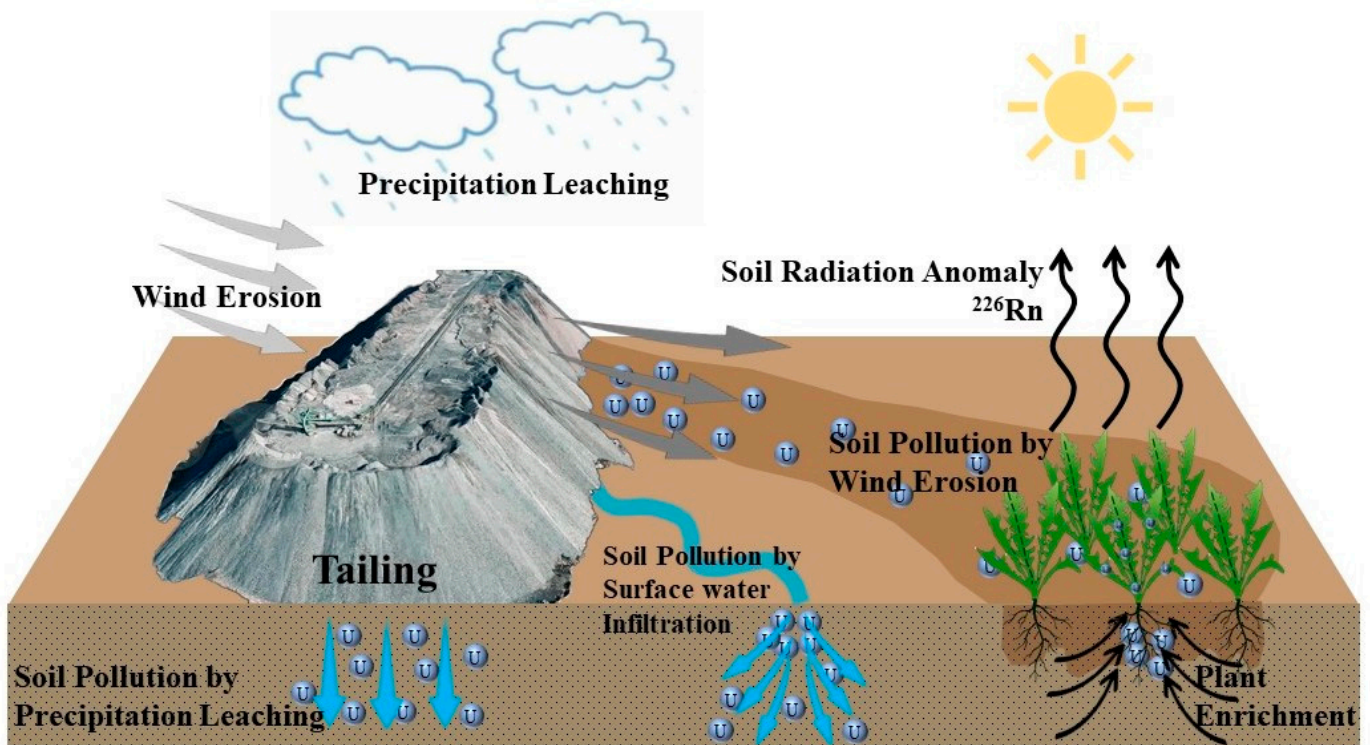
Figure 6. Soil pollution under wind erosion and precipitation leaching.

Open wastewater leakage can also cause soil pollution. For example, in a mine in the northern basin [98], due to the discharge of wastewater along the surface, heavy metals were carried downstream for more than 450 m but were mainly concentrated within 20 cm of the surface. The U content in the soil was 74.78–79.30 mg/kg, which was more than 27 times higher than the background value (2.72 mg/kg). In addition, other heavy metals have different degrees of pollution. The average exceedances of Cd, Cr, Cu, Mn, Ni, Pb and Zn were approximately 946.0, 5.7, 4.2, 1.7, 1.5, 4.7 and 4.4 times, respectively. Among them, Cd pollution is the most serious, and it is even worse than U pollution. Therefore, special attention should be given during production and remediation.

3.3. Environmental Impacts on the Groundwater Environment

Compared with soil, uranium ISL has a greater impact on groundwater. Similar to uranium deposits No. 737, No. 738 and No. 739 in Xinjiang [99,100], soil indicators remained within limits from mining to decommissioning. However, for groundwater, indicators were still in an abnormal state after years of decommissioning. Among them, $\sum$Fe (275 mg/L) and Mg^{2+} (252 mg/L) were more than 200 times higher than the background value, and SO_4^{2-}, U, Ca^{2+}, and NO_3^- also exceeded the standard numerous times. The pollution degree of groundwater varies with the mining method (Figure 7). Acid leaching has a significant influence on groundwater. The highest content elements in the groundwater of the acid-leaching mining area are usually SO_4^{2-}, $\sum$Fe, Ca^{2+}, Mg^{2+}, and U. Other heavy metals will also be leached into the groundwater. Although the concentration is relatively low, it still far exceeds the groundwater quality standard, posing a potential threat to the groundwater environment. The low pH of groundwater is another problem. Compared with acid leaching, CO_2 leaching is more friendly to the groundwater environment because the weakly alkaline environment leads to the precipitation of pollutants.
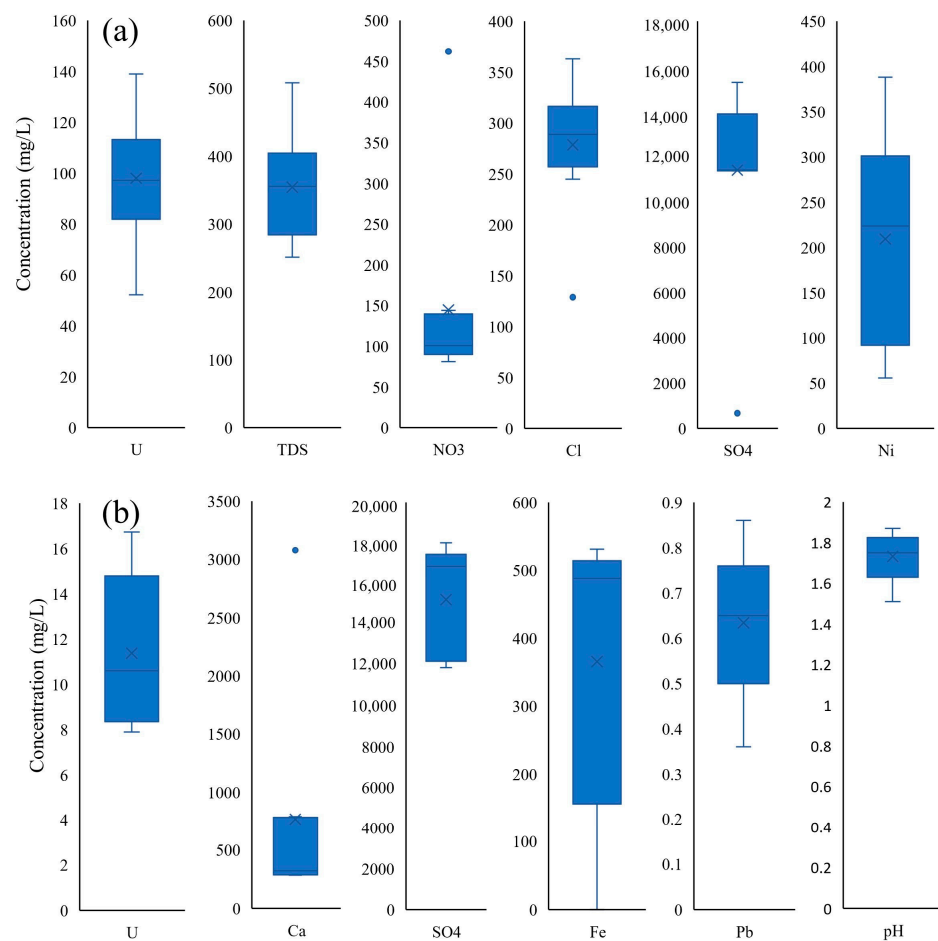
Figure 7. The statistical data of the main pollution ions in the acid-leaching (**a**) and CO_2-leaching (**b**) mining areas [89–91,100].

For example, in an acid-leaching area of a mixed mine in Ili (Table 3) [101], the pH of groundwater was 1.51–1.87, with an average of 1.73. The $\sum Fe$ pollution was the most serious, exceeding the background value by more than 2400 times; the content of SO_4^{2-} ranged from 11,900 to 18,000 mg/L, with an average of 15,200 mg/L, which was 120 times more than the background value. The content of U (11231 μg/L) was approximately 114 times that before mining (98 μg/L). Other elements, such as Ca, Mn, Ni, Zn, Pb, As, and Cd, all exceeded the background value by dozens or even hundreds of times. Similar to the $CO_2 + O_2$ leaching area in the same mine [101], the $\sum Fe$ in groundwater also decreased slightly after mining due to precipitation. The content of SO_4^{2-} was approximately 1/13 of the acid-leaching area, and Ca and Mg were approximately 1/2 and 1/3 of the acid-leaching area, respectively. The contents of other heavy metals were also significantly reduced. The U content increased, which was five times that of the acid-leaching area. However, CO_2 leaching can also lead to other chemical anomalies that are not available in the acid-leaching area. For example, the content of Cl^- (279 mg/L) was 3.2 times greater than that in the acid-leaching area (87 mg/L) and 14.5 times greater than the background value (19.43 mg/L). The HCO_3^- content was 148 mg/L, which was not detected in the acid-leaching area or before mining. In addition, ISL will use resin adsorption and nitrate leaching, resulting in nitrate exceeding the standard. Similar to a deposit in northwestern China, NO_3^- exceeded the background value by 140 times during the production period [80].
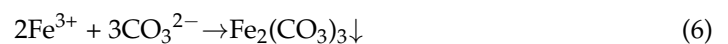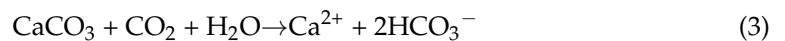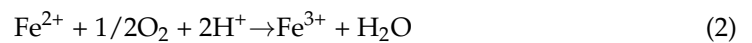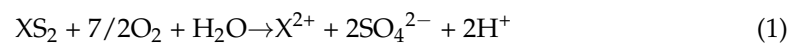
Table 3. Hydrochemical anomalies in some representative mining areas.

Location	Mining Method	pH	Concentration of Main Abnormal Elements (Background Value, mg/L)					Other Abnormal Indices	References
			Ca²⁺	Mg²⁺	U	SO₄²⁻	Fe		
Ili Basin Mine No. 737, 738 and 739	Acid (Decommissioned)	/	360 (17)	252 (1)	3.9 (<0.1)	3920 (127)	275 (<1)	K, Na, Re, Th, Mn, Cu	[99]
Inner Mongolia	CO₂ + O₂	7.62 (8.76)	16.10 (5.24)	8.17 (3.35)	43.05 (0.14)	272 (64)	0.09 (0.09)	TDS, HCO₃⁻, Cl⁻	[90,91]
Ili Basin (A mixed leaching mine)	Acid	1.73	766	342	11.2	15222	363	NO₃⁻, K, NaAl, Cu, Zn, Cd, Pb, Th, As	[101]
	CO₂ + O₂	7.32 (8.32)	342 (78)	99 (13)	60.0 (<0.1)	1139 (127)	0.04 (0.15)		
	Pollution halo	pH	Ca²⁺	Mg²⁺	U	SO₄²⁻	Fe	NO₃⁻	Cl⁻
	Vertically adjacent aquifers	7.55 (8.04)	104.3 (78)	23.8 (0.03)	0.03 (/)	216.8 (83.5)	3.13 (60)	0.73 (0.84)	75.1 (24.8)
	Upstream	7.43	91.5	28.6	0.026	202.4	2.38	2.81	42.35 [102]
Ili Basin	Mining area	3.42	266.5	232.62	6.28	4029.8	209.83	111.04	74.67
	200 m downstream	7.03	183.2	52.16	0.315	606.5	2.13	44.49	185.35
	1000 m downstream	7.5	81.6	27.36	0.054	109.4	0.57	0.06	52.48
	350 m from the side	7.37	121.1	33.01	0.022	414.5	1.13	0.06	77.25

Horizontally, the pollution halo is distributed along the groundwater flow direction, mainly concentrated downstream of the mine with a spread to both sides. The impact on the upstream groundwater is minor [81,91,102]. Vertically, it can barely affect the aquifer beyond the mining layer due to the dense aquifer [102]. Monitoring wells in some Ili mines [81,91,102] showed that the content of SO_4^{2-} downstream (606.5 mg/L) was 3 times that upstream (202.4 mg/L), U (315.34 μg/L) was 16 times that upstream (25.9 μg/L), and NO_3^- (144.49 mg/L) was 51 times that upstream (2.81 mg/L) (Table 3).

3.4. Chemical Clogging and Its Effects

Most of the sandstone-type uranium ores in China have high carbonate content, low permeability and low grade, which readily cause chemical clogging during ISL, resulting in the reduction of rock porosity and permeability [28,34,36,61,66]. The dissolution of rocks leads to a large increase in Ca^{2+}, Mg^{2+} and other heavy metal ions in groundwater. These ions react with the solvent to form $CaCO_3$, $CaSO_4$ or metal precipitates [28,103]. For iron or a kind of metal X, some of the main chemical reactions are as follows.

$$XS_2 + 7/2O_2 + H_2O \rightarrow X^{2+} + 2SO_4^{2-} + 2H^+ \tag{1}$$

$$Fe^{2+} + 1/2O_2 + 2H^+ \rightarrow Fe^{3+} + H_2O \tag{2}$$

$$CaCO_3 + CO_2 + H_2O \rightarrow Ca^{2+} + 2HCO_3^- \tag{3}$$

$$X^{2+} + CO_3^{2-} \rightarrow XCO_3\downarrow \tag{4}$$

$$X^{2+} + 2OH^- \rightarrow X(OH)_2\downarrow \tag{5}$$

$$2Fe^{3+} + 3CO_3^{2-} \rightarrow Fe_2(CO_3)_3\downarrow \tag{6}$$

$$Fe^{3+} + 3OH^- \rightarrow Fe(OH)_3\downarrow \tag{7}$$

Spatially, chemical clogging mainly occurs at the periphery of the injection well. The injection well is usually not clogged due to the continuous injection of the solvent. At locations far from the injection well, as the concentration of the solvent decreases or the pH increases, a precipitate will form in the solution (Figure 8a) [28,76]. The chemical precipitation moves along the groundwater and accumulates downstream, resulting in increased blockage along the groundwater flow direction (Figure 8b). This dissolution-precipitation-redissolution process leads to significant stratification of porosity around the injection well [68,76].

Temporally, chemical clogging has some hysteresis (Figure 8b). In the initial stage, due to the dissolution of the solvent, the porosity of the rock expands. Rock dissolution may increase porosity by 1–3% [68,104]. As the solvent content decreases, the pH decreases, and the metal cations react with CO_3^-, SO_4^{2-} or OH^- to form chemical clogging (Figure 8c) [103]. Clogging usually occurs after tens to hundreds of days if there is no human intervention [28].

Limited by chemical clogging, the spread of pollution halos is usually in a small area (Table 3, Figure 9). For high concentrations of pollutants (SO_4^{2-}, Fe, U, etc.) Along the groundwater flow direction, the migration distance can exceed 1000 m (Figure 9a). Other minor pollutants (Cl^-, NO_3^- and other heavy metals) are mainly concentrated within 200 m (Figure 9b). The maximum diffusion range to both sides was approximately 350 m [102]. In mining areas with a poor permeability coefficient, the effect of chemical clogging is more pronounced. The diffusion range of the pollution halo will be smaller. Similar to a mine in Qianjiadian [89], the deposit has low permeability (k < 0.2 m/d). The average diffusion rate of pollutants during mining was only 0.0843 m/d. After six years of mining, the diffusion range of the pollution halo was within 130 m, which basically controlled the area around the mine.
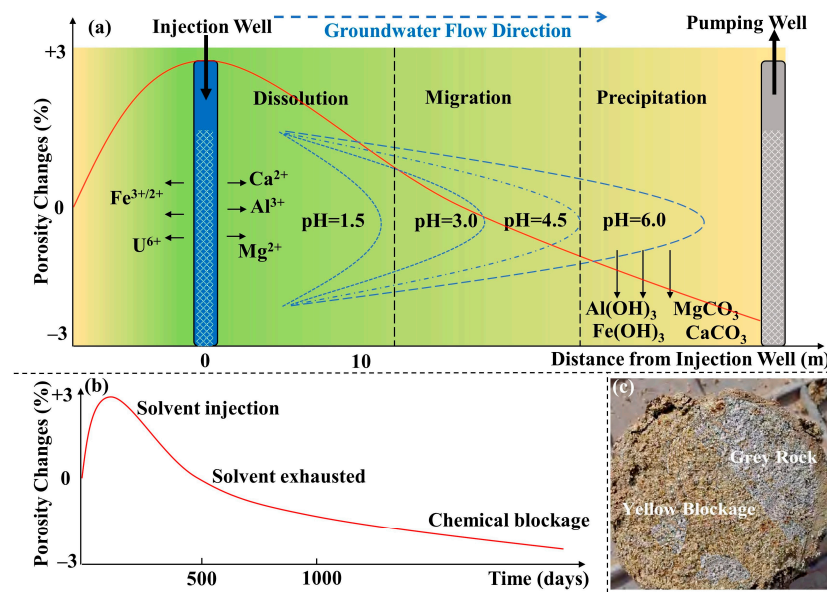
Figure 8. Chemical clogging during ISL. (**a**) Shows that chemical clogging occurs in space, while (**b**) shows that chemical clogging occurs over time; the red line shows the porosity changes; a positive value on the vertical axis indicates an increase, while a negative value indicates a decrease; (**c**) shows the yellow blockage in the gray rock, and the sample was collected in a decommissioned uranium mine in Northwest China.
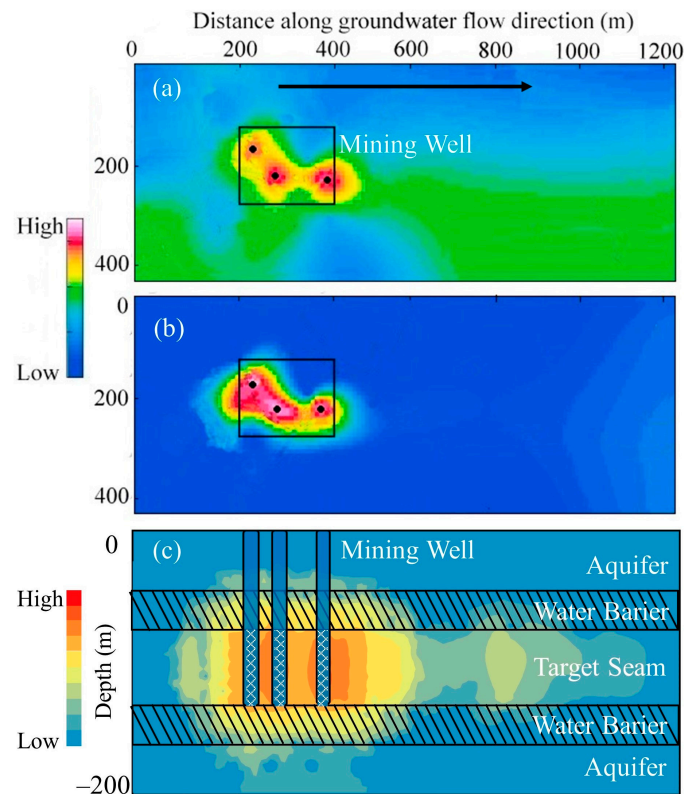

Figure 9. Schematic view of the groundwater pollution halo. The black square delineates the range of the mine, and the dots indicate the mining wells. (**a**) shows the pollution halo of primary high-concentration pollutants, such as SO_4^{2-}, Fe, and U; (**b**) shows the horizontal pollution halo of low-concentration pollutants, such as Cl^-, NO_3^- and other heavy metals; (**c**) shows the vertical pollution halo; the data were interpolated from the measurement of a decommissioned uranium mine in Northwest China.

3.5. Radiation Environment Impacts

Radon release and radiation exposure in uranium mines can result in radioactive abnormalities. The dissolution of the rock and soil by the solvent will result in the release of [226]Rn [105]. There are two main ways radon is released: evaporation of wastewater or waste liquid pools and precipitation of [226]Rn-content dust on the solid surface after uranium mine decommissioning [106,107]. The released content is mainly related to the concentration of [226]Rn in groundwater and leachate and the scale of the mine [106,107]. As in the No. 737 mine, mining produced approximately 1.22×10^{11} Bq of radon per 1 t of uranium produced. During the production of the Qian IV uranium mine in the Qianjiadian Basin, the [226]Rn released from the liquid collecting tank and the evaporation pond were 1.06×10^{-12} Bq/a and 1.48×10^{-7} Bq/a, respectively [100]. Due to the ventilation system and human management, radioactivity is typically controllable and will not cause a significant impact on the environment during production. However, for decommissioned uranium mines, the radioactivity of [226]Rn from heap leaching of tailings waste may far exceed the environmental limit. Similar to tailing in Liaoning Province, the [226]Rn radiation dose on the surface was approximately 3.14 Bq/(m^2·s), which was far beyond the management limits [108]. Another tailing's radiation dose exceeded the background value by 8.21 times but was only concentrated within 10 cm of the surface [109].

3.6. Plant Accumulation of Nuclides

Sandstone-type uranium deposits in northern China are mostly distributed in areas with poor soils. In these areas, most of the plants are herbs, such as Poaceae, Compositae or Leguminosae [110,111]. Since these plants are usually not used as food or economic crops and have good heavy metal tolerance, they have little impact on human or ecological health. Plants are usually used for geo-environmental restoration due to their good enrichment [82,112]. The U distribution in plants is usually root > stem > leaf [83,113]. Similar to tailing [109], the U content in plant roots was 0.18–42.7 mg/kg. For another tailing, the highest activity of uranium in plants in the mining area was 784.58 Bq/kg, 291 times higher than the background value. The content of heavy metals in plants was consistent with the distribution of the soil pollution halo. Additionally, affected by wind direction, the U content in plants behaves as follows: inside the mining area > southeast > northwest.

4. Mitigation of Environmental Impacts

4.1. Environmental Mitigation during Mining

With the increasing emphasis on environmental protection in recent years, various measures have been adopted in the ISL process to protect the geo-environment of mines. First, in terms of mining methods, an increasing number of mines use weak-alkaline leaching. $CO_2 + O_2$ solvent with mild chemical properties has begun to replace acid leaching [28]. In Ili, Ordos, Qianjiadian, etc., most of the mines use the weak-alkali method when the geological conditions allow [28,102]. Second, closed-loop mining methods were used in the mining processes. In Qianjiadian, a closed-loop treatment system of "leachate extraction-surface treatment-tail liquid treatment and reinjection" was adopted [89]. At the same time, an anti-seepage device was introduced into the production to treat wastewater, which basically achieved no wastewater discharge and no waste residue stacking [114]. Finally, the government usually formulated environmental norms in the mining process and made demands on land area, waste storage and treatment, quality and safety, etc. An environmental monitoring system must be established around the mine (Figure 10).
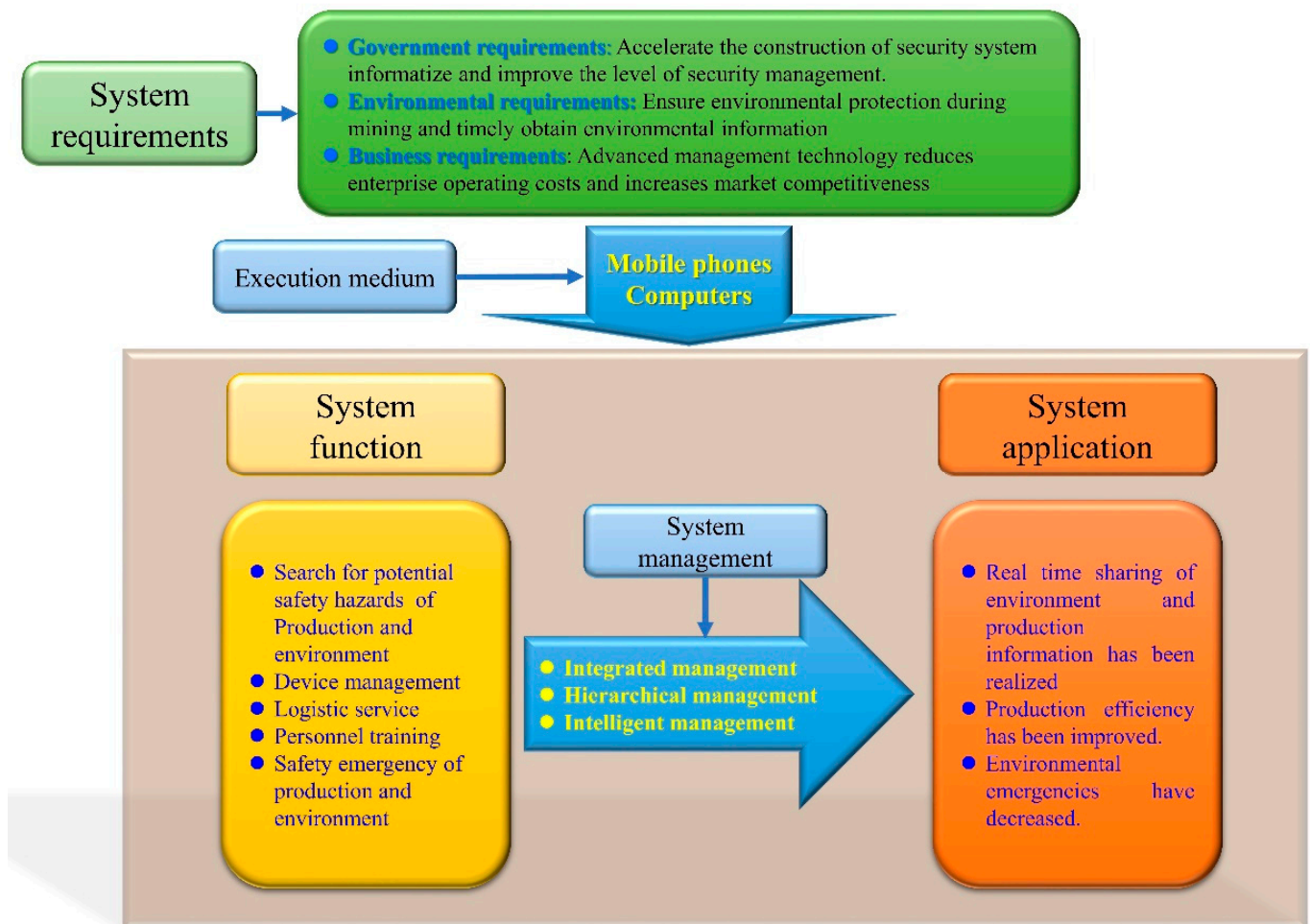
Figure 10. A demonstration security management system of ISL ore mine in Ordos.

4.2. Environmental Mitigation after Mining

At present, the main objects of remediation and treatment of decommissioned uranium mines in China are tailings storage, abandoned wells, wastewater and vegetation restoration. The assessment indicators of remediation and treatment usually focus on radiation reduction [79]. For tailings storage and abandoned wells, removal, landfill and plugging are the main methods for treatment, while for wastewater, artificial excretion is the main method [78]. The impact of the repaired mine on the surrounding environment can be reduced to a negligible level. Similar to the No. 440 uranium mine in Northeast China [115], there were 11 tailings heaps, 30 abandoned wells and tunnels, and more than 100,000 tons of waste residue after decommissioning. The average radiation dose in the area before treatment was approximately 557 nGy/h, 5 times more than the background value. By removing the waste and covering the site with compacted soil, the average environmental radiation dose after treatment was 60.54 nGy/h, which was even better than the level before mining. In addition, at the No. 781 mine in Henan Province, after decommissioning, U in groundwater exceeds the background value by 4.6 times and that in soil by 82 times. After the polluted water and soil were removed, 1.3 m thick planting soil was used for covering. Due to these remediation measures, the content of radioactive pollutants in water decreased by 82%, and the content of U in soil decreased by 98%, reaching the level before mining.

5. Environmental Management for Prospective Mining in the Future

5.1. Environmental Management during Uranium Mining

As described above, the pollution of uranium ISL is mainly concentrated in groundwater. In view of the difficult treatment of groundwater after pollution, it is necessary to strengthen groundwater protection during the mining process [77]. Measures can be taken from the following three phases. Before mining, the hydrogeological characteristics and chemical indicators of groundwater in the mining area should be investigated in detail, and the mine construction plan and decommissioning restoration goals should be formulated based on this. The drilling design of the mine should consider the groundwater flow direction and layout of wells from upstream to downstream, which can reduce the spread of the pollution halo to both sides. During operation, the volume of leaching solution extraction should be considered larger than the solvent injection. This can lead to negative pressure in the mining area and prevent pollutants from spreading outward. After the mine is exhausted, a monitoring system should be set up in the surrounding area, especially downstream. A periodic monitoring plan should be formulated to determine the range of pollution halo diffusion.

5.2. Environmental Management for Uranium Mine Closing

At present, the mainstream remediation methods of decommissioned uranium mines are to ensure the nonproliferation of pollution. Physical methods are used to isolate the contaminated area to prevent further damage to the nearby environment. However, U itself has not been repaired or removed, which should be considered in the future, especially under complex conditions. Conventional physical removal and chemical leaching are usually expensive and can easily cause secondary damage to the environment; phytoremediation is economical and environmentally friendly but is inefficient and limited by the capacity of enrichment [109,116,117]. These factors make it difficult to commercialize such methods on a large scale. Three methods can be considered for future application. The first is electric repair. Through electrodialysis, electromigration and other electrodynamic effects, uranium compounds migrate along the direction of the electric field and accumulate at the electrode, and then they can be removed by physicochemical methods (adsorption, ion exchange, precipitation, etc.) [75,84]. Especially in an acidic environment with a high iron content, the removal efficiency can reach 58–88% [75,84]. Second, microbial remediation can be considered. As a major participant in the biogeochemical cycle, microorganisms can reduce U(VI) to insoluble U(IV) precipitation through biological reduction, which can retard uranium migration in the environment [116,117]. Similar microbial reduction processes also exist in many uranium mineralization processes [118]. For example, with ethanol as the electron donor, the uranium concentration in groundwater can be reduced by more than 99.9% by microbial reduction [119]. Finally, for heavily polluted sites, PRB can be used for remediation. By placing the PRB wall downstream of the pollution halo, U can be removed by reacting with the medium in the wall. For the use of PRB, material selection is a challenge, such as zero-valent iron, activated carbon, slaked lime, quartz sand, etc. [120], which are all very promising materials but still need to be further verified in field trials.

6. Conclusions

In the context of China's carbon peak and carbon neutrality, the development of nuclear energy will reach its peak in the next few decades. As uranium is the main raw material for nuclear energy, environmental problems caused by mining should be taken seriously by government agencies. Sandstone-type uranium in northern China is mainly distributed in the Songliao Basin, Erlian Basin, Ordos Basin, Turpan–Hami Basin and Ili Basin from east to west. Most of the deposits are located in arid or semiarid regions with poor aquifer permeability, slow groundwater flow velocity and low hydraulic gradient. The type of uranium ore is usually dominated by pitchblende and is accompanied by pyrite, hematite, coal and organic matter. The main form of U is UO_2 in ore and uranyl

carbonate in groundwater. In situ leaching is the main method of sandstone-type uranium mining. The dissolution of the rock by the solvent will increase the porosity in a short period of time. However, as leaching continues, the rock crevice becomes clogged by metal precipitation, resulting in a decrease in porosity. Moreover, dissolution also leads to the release of other enriched metals, which cause groundwater pollution. The groundwater pollution in the mining area is mainly SO_4^{2-}, Fe and U. Other elements, such as Ca, Mg, NO_3^- and TDS, also have a significant increase. The pollution halo mainly diffuses along the groundwater flow direction. Due to chemical clogging, the diffusion range usually does not exceed 1000 m. Compared with groundwater, soil pollution is often much lighter. Soil chemical anomalies usually come from heap leaching and wind erosion of tailings. The heavy metals in the tailings can spread for several kilometers by wind, but they are mainly concentrated within 20 cm of the surface. Finally, uranium mining and heap leaching also cause radiation anomalies and radioactive enrichment in plants. Through treatment, decommissioned mines can have a negligible impact on the surrounding environment. Treatment methods are mainly physical partitioning, and pollutants have not been removed. At present, the attention and treatment of uranium tailings are still in their infancy. In the future, scholars should focus on the impact of decommissioned mines on the environment, including collecting more data for treatment assessment and providing statistical data support for environmental recovery. Economic and feasible methods should be widely reviewed to assess their practicality, such as electric remediation, microbial remediation or PRB, which are worth considering.

Author Contributions: All authors contributed to the study's conception and design. Material preparation, data collection and analysis were performed by Y.T. and Y.Z.; The draft of the manuscript was written by F.Z.; Figures and tables were made by J.H. and R.Z.; Proofreading and perfecting of the manuscript were performed by J.D. All authors commented on previous versions of the manuscript. All authors have read and agreed to the published version of the manuscript.

Institutional Review Board Statement: Not applicable.

Informed Consent Statement: Not applicable.

Data Availability Statement: Not applicable.

Conflicts of Interest: The authors have no relevant financial or non-financial interest to disclose.

References

1. Mallapaty, S. How China could be carbon neutral by mid-century. *Nature* **2020**, *586*, 482–483. [CrossRef] [PubMed]
2. Meng, M.; Yu, J. Chinese nuclear energy politics: Viewpoint on energy. *Energ. Source Part B* **2018**, *13*, 72–75. [CrossRef]
3. Dittmar, M. The end of cheap uranium. *Sci. Total Environ.* **2013**, *461*, 792–798. [CrossRef]
4. Xu, D.; Chi, G.; Nie, F.; Fayek, M.; Hu, R. Diversity of uranium deposits in China—An introduction to the Special Issue. *Ore. Geol. Rev.* **2021**, *129*, 103944. [CrossRef]
5. Jin, R.; Liu, H.; Li, X. Theoretical System of Sandstone-Type Uranium Deposits in Northern China. *J. Earth Sci.-China* **2022**, *33*, 257–277. [CrossRef]
6. Chen, Z.B.; Zhao, F.M.; Xiang, W.D.; Chen, Y.H. Uranium provinces in China. *Acta Geol. Sin.-Engl.* **2000**, *74*, 587–594.
7. Ilankoon, I.M.S.K.; Tang, Y.; Ghorbani, Y.; Northey, S.; Yellishetty, M.; Deng, X.; McBride, D. The current state and future directions of percolation leaching in the Chinese mining industry: Challenges and opportunities. *Min. Eng.* **2018**, *125*, 206–222. [CrossRef]
8. Hague, N.; Norgate, T. The greenhouse gas footprint of in-situ leaching of uranium, gold and copper in Australia. *J. Clean Prod.* **2014**, *84*, 382–390. [CrossRef]
9. Coral, T.; Placko, A.; Beaufort, D.; Tertre, E.; Bernier-Latmani, R.; Descostes, M.; De Boissezon, H.; Guillon, S.; Rossi, P. Biostimulation as a sustainable solution for acid neutralization and uranium immobilization post acidic in-situ recovery. *Sci. Total Environ.* **2022**, *822*, 153597. [CrossRef] [PubMed]
10. Pereira, R.; Antunes, S.C.; Marques, S.M.; Goncalves, F. Contribution for tier 1 of the ecological risk assessment of Cunha Baixa uranium mine (Central Portugal): I soil chemical characterization. *Sci. Total Environ.* **2008**, *390*, 377–386. [CrossRef]

11. Coral, T.; Descostes, M.; De Boissezon, H.; Bernier-Latmani, R.; de Alencastro, L.F.; Rossi, P. Microbial communities associated with uranium in-situ recovery mining process are related to acid mine drainage assemblages. *Sci. Total Environ.* **2018**, *628–629*, 26–35. [CrossRef] [PubMed]

12. Wanty, R.B.; Berger, B.R.; Plumlee, G.S.; King, T. Geoenvironmental models—An introduction. In *Deposit and Geoenvironmental Models for Resource Exploitation and Environmental Security*; Fabbri, A.G., Gaal, G., McCammon, R.B., Eds.; Springer: Matrahaza, Hungary, 2002; Volume 80, pp. 3–42.

13. Wang, M.; Ren, P.; Yan, G. The Updates on Geoenvironmental Study of Mineral Deposits in The Unite States and Propoed Strategy for China. *Adv. Earth Sci.* **2004**, *19*, 636–641.

14. Bussiere, B. Colloquium 2004: Hydrogeotechnical properties of hard rock tailings from metal mines and emerging geoenvironmental disposal approaches. *Can. Geotech. J.* **2007**, *44*, 1019–1052. [CrossRef]

15. Huang, J.; Huang, S. Regional metallogenic characteristics of China's uranium resources. *Uranium Geol.* **2005**, *21*, 129–138.

16. Nie, J.; Horton, B.K.; Saylor, J.E.; Mora, A.; Mange, M.; Garzione, C.N.; Basu, A.; Moreno, C.J.; Caballero, V.; Parra, M. Integrated provenance analysis of a convergent retroarc foreland system: U-Pb ages, heavy minerals, Nd isotopes, and sandstone compositions of the Middle Magdalena Valley basin, northern Andes, Colombia. *Earth-Sci. Rev.* **2012**, *110*, 111–126. [CrossRef]

17. Akhtar, S.; Yang, X.; Pirajno, F. Sandstone type uranium deposits in the Ordos Basin, Northwest China: A case study and an overview. *J. Asian Earth Sci.* **2017**, *146*, 367–382. [CrossRef]

18. Gomez, P.; Garralon, A.; Buil, B.; Turrero, M.J.; Sanchez, L.; De la Cruz, B. Modeling of geochemical processes related to uranium mobilization in the groundwater of a uranium mine (vol 300, pg 295, 2000). *Sci. Total Environ.* **2008**, *390*, 579. [CrossRef]

19. Cuvier, A.; Pourcelot, L.; Probst, A.; Prunier, J.; Le Roux, G. Trace elements and Pb isotopes in soils and sediments impacted by uranium mining. *Sci. Total Environ.* **2016**, *566*, 238–249. [CrossRef]

20. Bradshaw, P.; Lett, R. Geochemical-exploration for uranium using soils. *J. Geochem. Explor.* **1980**, *13*, 305–319. [CrossRef]

21. Cai, Y.; Zhang, J.; Li, Z.; Guo, Q.; Song, J.; Fan, H.; Liu, W.; Qi, F.; Zhang, M. Outline of Uranium Resources Characteristics and Metallogenetic Regularity in China. *Acta Geol. Sin.-Engl.* **2015**, *89*, 918–937. [CrossRef]

22. Li, Z.; Qin, M.; Fan, H.; Cai, Y.; Cheng, J.; Guo, D.; Ye, F.; Fan, G.; Liu, X. Main Progresses of Uranium Geology and Exploration Techniques for the Past Decade in China. *Bull. Mineral. Petrol. Geochem.* **2021**, *40*, 845–857.

23. Zhang, J. Progress and Outlook of Uranium Exploration in Meso-Cenozoic Basins in North China. *Uranium. Geol.* **2012**, *28*, 193–198.

24. Min, M.Z.; Chen, J.; Wang, J.P.; Wei, G.H.; Fayek, M. Mineral paragenesis and textures associated with sandstone-hosted roll-front uranium deposits, NW China. *Ore. Geol. Rev.* **2005**, *26*, 51–69. [CrossRef]

25. Min, M.Z.; Xu, H.F.; Chen, J.; Fayek, M. Evidence of uranium biomineralization in sandstone-hosted roll-front uranium deposits, northwestern China. *Ore. Geol. Rev.* **2005**, *26*, 198–206. [CrossRef]

26. Rong, H.; Jiao, Y.; Wu, L.; Wan, D.; Cui, Z.; Guo, X.; Jia, J. Origin of the carbonaceous debris and its implication for mineralization within the Qianjiadian uranium deposit, southern Songliao Basin. *Ore. Geol. Rev.* **2019**, *107*, 336–352. [CrossRef]

27. Shi, Z.; Chen, B.; Wang, Y.; Hou, M.; Jin, X.; Song, H.; Wang, X. A linkage between uranium mineralization and high diagenetic temperature caused by coal self-ignition in the southern Yili Basin, northwestern China. *Ore. Geol. Rev.* **2020**, *121*, 103443. [CrossRef]

28. Su, X.; Liu, Z.; Yao, Y.; Du, Z. Petrology, mineralogy, and ore leaching of sandstone-hosted uranium deposits in the Ordos Basin, North China. *Ore. Geol. Rev.* **2020**, *127*, 103768. [CrossRef]

29. Zhang, F.; Jiao, Y.; Wu, L.; Rong, H. Roles of dispersed organic matters in sandstone-type uranium mineralization: A review of geological and geochemical processes. *Ore. Geol. Rev.* **2021**, *139*, 104485. [CrossRef]

30. Fu, Y.; Wei, S.; Jin, R.; Li, J.; Ao, C. Current Status and Existing Problems of China' s Sandstone-type Uranium Deposits. *Acta Geol. Sin.* **2016**, *90*, 3519–3544.

31. Chen, X.; Romaniello, S.J.; Herrmann, A.D.; Hardisty, D.; Gill, B.C.; Anbar, A.D. Diagenetic effects on uranium isotope fractionation in carbonate sediments from the Bahamas. *Geochim. Cosmochim. Acta* **2018**, *237*, 294–311. [CrossRef]

32. Meunier, J.D.; TROUILLER, A.; Brulhet, J.; Pagel, M. Uranium and organic-matter in a paleodeltaic environment—The coutras deposit (gironde, france). *Chem. Geol.* **1988**, *70*, 189. [CrossRef]

33. Och, L.M.; Mueller, B.; Marz, C.; Wichser, A.; Vologina, E.G.; Sturm, M. Elevated uranium concentrations in Lake Baikal sediments: Burial and early diagenesis. *Chem. Geol.* **2016**, *441*, 92–105. [CrossRef]

34. Bonnetti, C.; Cuney, M.; Malartre, F.; Michels, R.; Liu, X.; Peng, Y. The Nuheting deposit, Erlian Basin, NE China: Synsedimentary to diagenetic uranium mineralization. *Ore. Geol. Rev.* **2015**, *69*, 118–139. [CrossRef]

35. Bonnetti, C.; Liu, X.; Mercadier, J.; Cuney, M.; Deloule, E.; Villeneuve, J.; Liu, W. The genesis of granite-related hydrothermal uranium deposits in the Xiazhuang and Zhuguang ore fields, North Guangdong Province, SE China: Insights from mineralogical, trace elements and U-Pb isotopes signatures of the U mineralisation. *Ore. Geol. Rev.* **2018**, *92*, 588–612. [CrossRef]

36. Qiu, J.; Mu, H.; Yu, X.; Rui, X.; Yang, Y.; Qiu, L. Identifying the principal factors controlling uranium enrichment: Semi-quantitative mineralogy and geochemistry of the sandstone-type Qianjiadian uranium deposit, northeast China. *Ore. Geol. Rev.* **2022**, *144*, 104807. [CrossRef]

37. Chen, J.; Chen, P.; Yao, D.; Huang, W.; Tang, S.; Wang, K.; Liu, W.; Hu, Y.; Zhang, B.; Sha, J. Abundance, Distribution, and Modes of Occurrence of Uranium in Chinese Coals. *Miner.-Basel.* **2017**, *7*, 239. [CrossRef]

38. Chen, J.; Bai, Q.; Tian, Y.; Lu, Y.; Niu, J.; Shi, L.; Yang, Y. Discussion on Prospecting Directions of Uranium Deposit in Coal Measure Strata in the North of Yining Area, Xinjiang. *Uranium. Geol.* **2021**, *37*, 160–170.

39. Huang, W.; Wan, H.; Finkelman, R.B.; Tang, X.; Zhao, Z. Distribution of uranium in the main coalfields of China. *Energ. Explor. Exploit.* **2012**, *30*, 819–835. [CrossRef]

40. Liu, X.; Yu, R.; Cao, H.; Zhu, Q.; Wang, S.; Yang, J. Metallogenic conditions of sandstone uranium deposits in the coal-bearing area on the southeastern margin of Ordos basin. *Coal. Geol. Explor.* **2018**, *46*, 26–32.

41. Tang, C.; Zhu, Q.; Feng, X.; Chen, Y.; Li, G.; Chen, L.; Liu, X.; Liu, X.; Hu, P. REE geochemical study on Dongsheng sandstone uranium deposit, Inner Mongolia, China. *Acta Mineral. Sin.* **2017**, *37*, 121–131.

42. Wang, Z.; Cao, S.; Pan, J.; Guan, T.; Zhang, G. Trace element geochemistry of No. 511 uranium ore deposit in Xinjiang. *Miner. Depos.* **2005**, *24*, 409–415.

43. Xue, W.; Xue, C.; Chi, G.; Peng, Y.; Wang, K. Trace Element and REE Geochemical Characteristics of Sandstone-type Uranium Deposit in the Dongsheng Area of the Ordos Basin, China. *Geoscience* **2010**, *24*, 776–784.

44. Nie, F.; Yan, Z.; Feng, Z.; Li, M.; Xia, F.; Zhang, C.; Wang, Y.; Yang, J.; Kang, S.; Shen, K. Genetic models and exploration implication of the paleochannel sandstone-type uranium deposits in the Erlian Basin, North China—A review and comparative study. *Ore. Geol. Rev.* **2020**, *127*, 103821. [CrossRef]

45. Wang, S.Y.; Cheng, Y.H.; Xu, D.H.; Miao, P.S.; Jin, R.S.; Zhang, T.F.; Xu, Z.L.; Cheng, X.Y.; Zhao, L.; Li, C.H.; et al. Late Cretaceous-Cenozoic tectonic-sedimentary evolution and U-enrichment in the southern Songliao Basin. *Ore. Geol. Rev.* **2020**, *126*, 103786. [CrossRef]

46. Liu, Z.; Yang, B.; Zhao, X.; Wang, T. Mineral Ingredient and Geochemical Characteristics of Uranium Mineralization at Shihongtan Uranium Deposit, Turpan-Hami Basin. *Xinjiang Geol.* **2018**, *36*, 257–261.

47. Chen, G.; Sun, Z.; Nie, F.; Li, C.; Zhen, Y.; Zhou, Z. Hydrogeochemical characteristics of the sandstone-hosted uranium mineralization in northern Ordos Basin, China. *Ore. Geol. Rev.* **2020**, *126*, 103769. [CrossRef]

48. Ren, J.; Xia, Y.; Zhang, Z.; Lin, Y. Study on the Hydrological Conditions of Qianjiadian Sandstone Type Uranium for In-situ Leaching Mining in Songliao Basin. *Uranium. Min. Metall.* **2022**, *41*, 21–29. [CrossRef]

49. Cao, L.; Qiao, H.; Zhou, W.; Wu, Z. Analysis on affecting factors of metallogenic difference in the southern ore belt of Shihongtan uranium deposit. *World Nucl. Geosci.* **2018**, *35*, 77–83.

50. Yue, S.; Wang, G. Relationship between the hydrogeochemical environment and sandstone-type uranium mineralization in the Ili basin, China. *Appl. Geochem.* **2011**, *26*, 133–139. [CrossRef]

51. Qiao, H.; Song, Z.; Zhang, J. The effect of gas from the groundwater in the forming of uranium deposit at Shihongtan. *Uranium. Geol.* **2009**, *25*, 222–227.

52. Qiao, H.; Zhang, T.; Zhang, F.; Shang, G.; Song, Z. Hydrogeochemical characteristics of Shihongtan uranium deposit in Turpan-Hami basin. *Uranium. Geol.* **2005**, *21*, 345–352.

53. Li, Y.; Li, S.; Ren, M. Study on the Relationship Between Hydrogeological Models with Uranium Mineralization, Take Uranium of Northern Ili Basin as an Example. *Xinjiang Geol.* **2019**, *37*, 107–111.

54. Lin, X.; Li, X.; Liu, W.; Xu, Q. Hydrogeological Conditions of Uranium Mineralization in Yihegaole Area, Erlian Basin. *Uranium. Geol.* **2020**, *36*, 464–476.

55. Lin, X.; Liu, H.; Wang, Z.; Hao, W. Hydrogeochemical Modeling Study on Mengqiguer Uranium Deposit in Yili Basin. *Uranium. Geol.* **2017**, *33*, 346–355.

56. Chen, G.; Sun, Z.; Wang, G.; Liu, J. The isotopic and chemical characteristics of groundwater from Shihongtan uranium deposit and its surrounding area. *Geochim. Cosmochim. Acta* **2009**, *73*, A212.

57. Chen, Z.; Man, A.; Chen, X.; Xiong, Y.; Shao, J.; Wang, L.; Sun, P. Relationship Between Hydrogeology and Sandstone Uranium Mineralization in Sedimentary Basin: A Case Study of Sandstone Uranium Survey in the Kailu Depression of the Songliao Basin. *Geotecton. Metallog.* **2021**, *45*, 1174–1184.

58. Iskander, F.Y. Assessment of trace elements in honey produced on uranium mining reclaimed land. *Sci. Total Environ.* **1996**, *192*, 119–122. [CrossRef]

59. Yao, Y.; Liu, D.; Yan, T. Geological and hydrogeological controls on the accumulation of coalbed methane in the Weibei field, southeastern Ordos Basin. *Int. J. Coal. Geol.* **2014**, *121*, 148–159. [CrossRef]

60. Gang, W.; Fa, Z.; Dapeng, H.; Ji'An, L. Analysis of In-situ Leaching Feasibility in Northern Belt of Shihongtan Uranium Deposits in Xinjiang Turpan. *J. East China Inst. Technol. (Nat. Sci. Ed.)* **2015**, *38*, 58–63.

61. Qiu, W.; Liu, Z.; Yang, Y.; Weng, H.; Jia, Y.; Wu, J.; Li, H.; Liu, S.; Wu, J. Reactive transport numerical modeling of $CO_2 + O_2$ in-situ leaching in sandstone-type uranium ore. *Sci. Sin. (Technol.)* **2022**, *52*, 627–638.

62. Hao, J. Application of Geochemical Model in the Prediction of Sandstone-Type Uranium Deposits in Eastern Erlian Basin. *Uranium. Geol.* **2013**, *29*, 24–30, 46.

63. Lin, N.; Shutao, H.; Guisheng, Y. The characteristics of uranium mineralization and cenesis of Nuheting uranium deposit in Erlian basin inner mongolian. *China Nucl. Sci. Technol. Rep.* **1995**, *00*, 1005–1017.

64. Zhang, P.; Nie, F.; Zhang, C.; Zhang, H.; Dong, Y.; Zhang, X. Characteristics and Its Implications for the Mineralization of the Sandstone from Uranium-Bearing Target Layer in Langka, Yili Basin. *Sci. Technol. Eng.* **2018**, *18*, 29–38.

65. Jiao, Y.; Chen, A.; Wang, M.; Wu, L.; Yuan, H.; Yang, Q.; Zhang, C.; Xu, Z. Genetic Analysis of the Bottom Sandstone of Zhiluo Formation, Northeastern Ordos Basin:Predictive base of spatial orientation of sandstone-type uranium deposit. *Acta Sedimentol. Sin.* **2005**, *23*, 371–379.

66. Ma, X.; Wang, K.; Jin, R.; Li, J.; Zhou, H.; Yang, H. Characteristics of fluid inclusions in the sandstone-hosted Qianjiadian uranium deposit, southwest Songliao Basin, northeastern China: Implications for the nature and evolution of ore-forming fluids. *Resour. Geol.* **2022**, *72*, e12281. [CrossRef]

67. Min, M.; Peng, X.; Zhou, X.; Qiao, H.; Wang, J.; Zhang, L. Hydrochemistry and isotope compositions of groundwater from the Shihongtan sandstone-hosted uranium deposit, Xinjiang, NW China. *J. Geochem. Explor.* **2007**, *93*, 91–108. [CrossRef]

68. Zhao, L.; Deng, J.; Xu, Y.; Zhang, C. Mineral alteration and pore-plugging caused by acid in situ leaching: A case study of the Wuyier uranium deposit, Xinjiang, NW China. *Arab. J. GeoSci.* **2018**, *11*, 707. [CrossRef]

69. Huang, G.; Yu, F.; Pan, J.; Cheng, Z.; Wu, D.; Xue, W.; Song, T.; Li, S. Genesis of pyrite from the Mengqiguer uranium deposit in Ili Basin of Xinjiang and its implication for mineralization. *Geol. China* **2021**, *48*, 507–519.

70. Zhang, X.; Nie, F.; Xia, F.; Zhang, C.; Feng, Z.; Ullah, R.; Zhang, P. Provenance constraints on the Xishanyao Formation, southern Yili Basin, northwest China: Evidence from petrology, geochemistry, and detrital zircon U-Pb geochronology. *Can. J. Earth Sci.* **2018**, *55*, 1020–1035. [CrossRef]

71. Gao, B.; Sun, Z.X.; Wang, G.C. Geochemical characteristics of the Shihongtan uranium deposit in Turpan-Hami basin, West Clehina. *Geochim. Cosmochim. Acta* **2008**, *72*, A292.

72. Liu, H.; Ding, B.; Liu, Z.; Zhang, X.; Pan, C. Genesis of strong kaolinization in ore-bearing sandstone from Mengqiguer uranium deposit, Yili Basin, China. *Acta Mineral. Sin.* **2017**, *37*, 40–48.

73. Zhu, X.; Wang, Y.; Wang, Z.; Zhang, C.; Liu, J. Trace element geochemistry of sandstone-type uranium deposits in dongsheng area. *Geol. -Geochem.* **2003**, *31*, 39–45.

74. Li, R.; Liu, C.; Li, Z.; Liang, L. Geochemical Characteristics of Trace Elements of Sandstone-type Uranium Deposit in Huhe Area, Bayintala Depression. *Uranium. Geol.* **2015**, *31*, 438–444, 466.

75. Kong, L.; Su, M.; Mai, Z.; Li, H.; Diao, Z.; Xiong, Y.; Chen, D. Removal of uranium from aqueous solution by two-dimensional electrosorption reactor. *Environ. Technol. Innov.* **2017**, *8*, 57–63. [CrossRef]

76. Zhao, L.; Cai, C.; Jin, R.; Li, J.; Li, H.; Wei, J.; Guo, H.; Zhang, B. Mineralogical and geochemical evidence for biogenic and petroleum-related uranium mineralization in the Qianjiadian deposit, NE China. *Ore. Geol. Rev.* **2018**, *101*, 273–292. [CrossRef]

77. Zhu, Q.; Yu, R.; Feng, X.; Li, J.; Sima, X.; Tang, C.; Xu, Z.; Liu, X.; Si, Q.; Li, G.; et al. Mineralogy, geochemistry, and fluid action process of uranium deposits in the Zhiluo Formation, Ordos Basin, China. *Ore. Geol. Rev.* **2019**, *111*, 102984. [CrossRef]

78. Qiu, G. Discussion on radioactive environmental impact assessment for the decommission of uranium mining and milling facilities. *Uranium. Geol.* **2008**, *24*, 188–192.

79. Mao, Y.; Yong, J.; Liu, Q.; Wu, B.; Chen, H.; Hu, Y.; Feng, G. Heavy Metals/Metalloids in Soil of a Uranium Tailings Pond in Northwest China: Distribution and Relationship with Soil Physicochemical Properties and Radionuclides. *Sustainability* **2022**, *14*, 5315. [CrossRef]

80. Wang, Q.; Hu, N.; Ding, D.; Zhang, G.; Hu, E.; Zhang, H.; Yang, Y.; Jiang, X. Removal of NO_3~–N From Polluted Groundwater in Decommissioned Mining Area in an In-situ Leach Uranium Mine by Denitrifying Bacteria Bioreactor. *At. Energy Sci. Technol.* **2013**, *47*, 1300–1306.

81. Dong, Y.; Xie, Y.; Li, G.; Zhang, J. Efficient natural attenuation of acidic contaminants in a confined aquifer. *Environ. Earth Sci.* **2016**, *75*, 595. [CrossRef]

82. Wang, Z.; Qin, H.; Wang, J. Accumulation of uranium and heavy metals in the soil-plant system in Xiazhuang uranium ore field, Guangdong Province, China. *Environ. Geochem. Health* **2019**, *41*, 2413–2423. [CrossRef] [PubMed]

83. Yu, X.; Song, Y.; Wei, G.; Yu, G.; Gao, Y.; Xiao, F.; Ma, M. Pollution Characteristics of U and Th in Soil and Plant Screening in Light Rare Earth Tailings. *Environ. Sci. Technol.* **2020**, *43*, 26–30.

84. Li, M.; Gao, F.; Zhang, X.; Lv, S.; Huang, J.; Wu, X.; Fang, Q. Recovery of uranium from low-grade tailings by electro-assisted leaching. *J. Clean Prod.* **2020**, *271*, 122639. [CrossRef]

85. Brown, P.L.; Guerin, M.; Hankin, S.I.; Lowson, R.T. Uranium and other contaminant migration in groundwater at a tropical Australian Uranium Mine. *J. Contam. Hydrol.* **1998**, *35*, 295–303. [CrossRef]

86. Wu, Y.; Li, J.; Wang, Y.; Xie, X. Variations of uranium concentrations in a multi-aquifer system under the impact of surface water-groundwater interaction. *J. Contam. Hydrol.* **2018**, *211*, 65–76. [CrossRef]

87. Atkins, M.L.; Santos, I.R.; Perkins, A.; Maher, D.T. Dissolved radon and uranium in groundwater in a potential coal seam gas development region (Richmond River Catchment, Australia). *J. Environ. Radioact.* **2016**, *154*, 83–92. [CrossRef]

88. Shi, S.; Tang, X.; Yang, Y.; Liu, Z. Biological effects of uranium in water, soil and rice in uranium deposits in southern China. *J. Radioanal. Nucl. Ch.* **2021**, *328*, 507–517. [CrossRef]

89. Zhang, Y.; Ma, L.; Zhang, B.; Li, X. Discussion the influence of the in-suit leaching process on groundwater environment in a low permeability uranium deposit. *Uranium. Min. Metall.* **2017**, *36*, 75–86. [CrossRef]

90. Dong, H.; Li, X.; Zhang, B. Experimental study on $CO_2 + O_2$ in-suit leaching of uranium in a uranium mine in Inner Mongolia. *Uranium. Min. Metall.* **2019**, *38*, 8–13. [CrossRef]

91. Long, H.; Shen, H.; He, X.; Chen, L.; Zuo, W. Practice of groundwater control in acid in-suit leaching of uranium. *Uranium. Min. Metall.* **2017**, *36*, 58–65. [CrossRef]

92. Zhang, W.; Liu, H.; Fan, X.; Zhuo, Z.; Guo, Y. Removal of uranium from aqueous solution by a permeable reactive barrier loaded with hydroxyapatite-coated quartz sand: Implication for groundwater remediation. *Geochemistry* **2020**, *80*, 125545. [CrossRef]

93. Kirsch, K.; Navarre-Sitchler, A.K.; Wunsch, A.; McCray, J.E. Metal Release from Sandstones under Experimentally and Numerically Simulated CO2 Leakage Conditions. *Environ. Sci. Technol.* **2014**, *48*, 1436–1442. [CrossRef] [PubMed]

94. Youlton, B.J.; Kinnaird, J.A. Gangue-reagent interactions during acid leaching of uranium. *Min. Eng.* **2013**, *52*, 62–73. [CrossRef]

95. Tan, K.; Li, C.; Liu, J.; Qu, H.; Xia, L.; Hu, Y.; Li, Y. A novel method using a complex surfactant for in-situ leaching of low permeable sandstone uranium deposits. *Hydrometallurgy* **2014**, *150*, 99–106. [CrossRef]

96. Ji, H.; Zhou, Y.; Sun, Z.; Yang, Y. Analysis of and Discussion on $CO_2 + O_2$ In-situ Leaching of Uranium Process at Mengqiguer Deposit. *Nonferrous Met. (Extr. Metall.)* **2018**, *10*, 55–59.

97. Guo, Y.; Wei, W.; Cheng, L.; Li, J.; Han, X. U, Th and [226]Ra Vertical Migration in Sub-Clay From an Uranium Tailings Impoundment. *Radiat. Prot.* **2005**, *25*, 24–30.

98. Yao, F.; Xiaolei, J.; Liangshu, X. Contamination Assessment to a Uranium Mine in China Based on the Fault Tree Analysis. *J. Univ. Souht China (Sci. Technol.)* **2015**, *29*, 22–26. [CrossRef]

99. Tian, X.; Diao, C. Analysis of environmental impact about in-situ leaching uranium mines of Xinjiang and measures of pollution prevention. *Uranium. Min. Metall.* **2010**, *29*, 29–32. [CrossRef]

100. Zhong, J.; Zhang, Z.; Xia, M. Research on in-suit leaching technological mineralogy in Qian IV block of Qianjiadian uranium deposit in southern Songliao Basin. *Miner. Explor.* **2022**, *13*, 192–199. [CrossRef]

101. He, C.; Tan, K.; Li, Y.; Liu, Z.; Zhang, Q.; Li, D.; Liu, Z. Pollution characteristics and mechanism of groundwater of acid and CO2 In-situ leaching mining area of uranium deposit in Xinjiang, China. *Nonferrous Met. (Extr. Metall.)* **2021**, *6*, 53–59.

102. Zuo, W.; Tan, K. The characteristics of groundwater contamination of a decommissioned wellfield in some in suit leaching uranium min, Xinjiang, China. *J. Univ. South China (Sci. Technol.)* **2014**, *28*, 28–34. [CrossRef]

103. Zeng, S.; Shen, Y.; Sun, B.; Zhang, N.; Zhang, S.; Feng, S. Pore structure evolution characteristics of sandstone uranium ore during acid leaching. *Nucl. Eng. Technol.* **2021**, *53*, 4033–4041. [CrossRef]

104. Cheng, Y.; Hu, X.; Kong, Y.; Dong, Y.; Guo, J.; Wang, L.; Wang, J. Imaging acidic contaminants in a confined aquifer using electromagnetic geophysical method constrained by hydrochemical data. *J. Hydrol.* **2022**, *609*, 127704. [CrossRef]

105. Darby, S.C.; Whitley, E.; Howe, G.R.; Hutchings, S.J.; Kusiak, R.A.; Lubin, J.H.; Morrison, H.I.; Tirmarche, M.; Tomasek, L.; Radford, E.P.; et al. Radon and cancers other than lung-cancer in underground miners—A collaborative analysis of 11 studies. *Jnci.-J. Natl. Cancer I* **1995**, *87*, 378–384. [CrossRef]

106. Bernhard, S.; Legac, J.A.; Zettwoog, P.R.; Sequin, H. Occupational exposure to rn in non-uranium mines in the european-community. *Health Phys.* **1985**, *49*, 999–1002. [PubMed]

107. Lespukh, E.; Stegnar, P.; Yunusov, M.; Tilloboev, H.; Zyazev, G.; Kayukov, P.; Hosseini, A.; Stromman, G.; Salbu, B. Assessment of the radiological impact of gamma and radon dose rates at former U mining sites in Tajikistan. *J. Environ. Radioact.* **2013**, *126*, 147–155. [CrossRef]

108. Hu, L.; Guo, D.; Li, Z.; Li, Y.; Zhang, N. Design of cover system for decommissioning of uranium mill tailings pond. *Uranium. Min. Metall.* **2021**, *40*, 70–75. [CrossRef]

109. Jiang, X.; Yan, D.; He, Y.; Zhao, X.; Ding, K. Survey of radioactivity level of uranium in plants within uranium tailings waste backfilling area. *Radiat. Prot.* **2018**, *38*, 132–136.

110. Luo, Y.; Peng, Q.; Li, K.; Gong, Y.; Liu, Y.; Han, W. Patterns of nitrogen and phosphorus stoichiometry among leaf, stem and root of desert plants and responses to climate and soil factors in Xinjiang, China. *Catena* **2021**, *199*, 105100. [CrossRef]

111. Lu, L.; Mao, L.; Yang, T.; Ye, J.; Liu, B.; Li, H.; Sun, M.; Miller, J.T.; Mathews, S.; Hu, H.; et al. Evolutionary history of the angiosperm flora of China. *Nature* **2018**, *554*, 234. [CrossRef]

112. Feng, Y.; Hu, X.; Lu, L.; Zhou, W.; Zhang, Y. The Migration of U and Th in the Tailings-plants System. *Earth Environ.* **2014**, *42*, 201–206.

113. Yan, D.; Ding, K.; He, Y.; Fan, L.; Zuo, R.; Jiang, X. Uptake of uranium by plants growing around an old uranium mill tailing in northeast China. *Fresen. Environ. Bull* **2018**, *27*, 3102–3106.

114. Tang, Q.; Yang, J.; Tian, C.; Jin, R.; Li, J.; Ao, C.; Zhang, Z. In-situ leaching for sandstone type uranium deposit in Songliao basin and ecological conservation. *North China Geol.* **2016**, *39*, 136–139.

115. Long, B.; Lu, X.; Li, Y.; Tao, J. Decommissioning governance and significance of geological exploration engineering facilities of a military uranium mine in Heilongjiang Province. *Jilin Geol.* **2021**, *40*, 77–79.

116. Gavrilescu, M.; Pavel, L.V.; Cretescu, I. Characterization and remediation of soils contaminated with uranium. *J. Hazard Mater.* **2009**, *163*, 475–510. [CrossRef]

117. Lovley, D.R.; Phillips, E.; Gorby, Y.A.; Landa, E.R. Microbial Reduction of Uranium. *Nature* **1991**, *350*, 413–416. [CrossRef]

118. Borch, T.; Kretzschmar, R.; Kappler, A.; Van Cappellen, P.; Ginder-Vogel, M.; Voegelin, A.; Campbell, K. Biogeochemical Redox Processes and their Impact on Contaminant Dynamics. *Environ. Sci. Technol.* **2010**, *44*, 15–23. [CrossRef]

119.	Wu, W.; Carley, J.; Gentry, T.; Ginder-Vogel, M.A.; Fienen, M.; Mehlhorn, T.; Yan, H.; Caroll, S.; Pace, M.N.; Nyman, J.; et al. Pilot-scale in situ bioremedation of uranium in a highly contaminated aquifer. 2. Reduction of U(VI) and geochemical control of U(VI) bioavailability. *Environ. Sci. Technol.* **2006**, *40*, 3986–3995. [CrossRef]

120.	Xiao, J.; Pang, Z.; Zhou, S.; Chu, L.; Rong, L.; Liu, Y.; Li, J.; Tian, L. The mechanism of acid-washed zero-valent iron/activated carbon as permeable reactive barrier enhanced electrokinetic remediation of uranium-contaminated soil. *Sep. Purif. Technol.* **2020**, *244*, 116667. [CrossRef]